Chapter III-6

Resonant Molecular Optics

B. DICK

Max Planck Institut für biophysikalische Chemie
Karl-Friedrich-Bonhoeffer Institut, Abteilung Laserphysik
Postfach 2841, D-3400 Göttingen, Federal Republic of Germany

R. M. HOCHSTRASSER

Department of Chemistry
University of Pennsylvania
Philadelphia, Pennsylvania 19104

H. P. TROMMSDORFF

Laboratoire de Spectrométrie Physique associé au C.N.R.S.;
Université Scientifique, Technologique, et Médicale de Grenoble
BP 87, 38402 St. Martin d'Hères Cedex, France

I. INTRODUCTION

Molecular optics concerns the study of nonlinear processes and materials derived from molecular systems. The existence of a wide range of molecular structures gives rise to a correspondingly large variety of optical transitions. These transitions, or resonances, determine the nature of the responses of the

system to electromagnetic fields; hence their detailed study is of paramount importance to the development of a fuller understanding of the nonlinear properties. For some purposes it is advantageous to optimize the nonlinear response in the transparent regime of the material. In such a case the losses are minimal and the response times are shortest. However, enormous enhancements of the nonlinear signals occur when the incident electromagnetic field frequencies match those of the optical transitions. In order to understand the responses in such cases, it is necessary to have detailed knowledge of both the optical transitions and the dynamical processes that can be undergone by the excited states. This special case of *resonant molecular optics* is the subject of the present chapter.

In order to lay the basis for later applications to specific systems, Section II consists of a survey of the structural and dynamical properties of molecular condensed matter. Both the vibrational and the electronic resonances of molecular solids are discussed, as are the effects on them of intermolecular interactions, energy transfer, charge transfer, and disorder. Section III contains the theoretical foundation of the resonant nonlinear responses, from which later results can be deduced. Density matrix methods that can be used to describe the interaction of molecules with both weak and strong laser fields are developed in this section, which relies heavily on previous fundamental work on the resonant nonlinear response (Bloembergen, 1965; Butcher, 1965; Hellwarth, 1977; Flytzanis, 1975). In resonant nonlinear experiments, energy is transferred from the electromagnetic field to the medium, so in Section III we also consider the optics of each experiment in terms of complex wave vectors including all the relevant absorption coefficients. Section IV is the main part of the chapter, consisting of a review of resonant nonlinear optical experiments chosen to illustrate the variety of molecular responses and systems that have been studied during the past few years. The nonlinear optical properties and spectroscopic transitions can usually be studied by the time-domain or frequency-domain methods. A part of our interest has been to establish experimental and theoretical relationships between these two approaches, and such comparisons are brought out whenever possible.

II. STRUCTURAL AND DYNAMICAL PROPERTIES OF MOLECULAR SYSTEMS

A. Electronic States and Transitions

The linear absorption strengths of electronic transitions in molecules range over ~ 12 orders of magnitude. The weakest are the singlet-to-triplet transitions, which may have f values as low as 10^{-12}, and the strongest spin-

allowed transitions have $f \approx 1$. The range of nonlinear interaction strengths is even greater—10^{24} for second-order and 10^{36} for third-order processes. Even the symmetry-allowed transitions of a molecule cover a range of f values that for an aromatic hydrocarbon might be as much as two orders of magnitude. Thus it is apparent that the extent of resonant enhancement of optical processes is very much dependent on the specific nature of the resonant state; for example, it is quite possible to have an exact resonance with a weak transition and yet have the signal dominated by nonresonant background effects. However, the extent of the chemical and structural changes that occur on electronic excitation is not necessarily related to the transition strength. For example, large changes in permanent dipole moment are known to occur for both weak and strong transitions.

The most common types of molecular excited states involve two-electron configurations of the type $\pi\pi^*$, $\sigma\pi^*$, and $n\pi^*$, or the excited electron is moved to another region of the molecule, leaving behind a positive center, to form a charge-transfer state. The low-energy states of aromatic and polyene molecules are of $\pi\pi^*$ type, whereas molecules having valence-shell electrons that are nonbonding frequently have low-energy $\sigma\pi^*$, $n\pi^*$, or charge-transfer states. Aromatic molecules and polyenes are often approximately centrosymmetric, such that their states can be classified as even (g) and odd (u) functions of the electronic coordinates. The aromatics usually have the u states at lowest energy, but there are many exceptions to this, including biphenyl (Whiteman *et al.*, 1973) and biphenylene (Hochstrasser and McAlpine, 1966; McAlpine, 1968), both of which have low-energy g states. Polyenes longer than three double bonds generally have a g state at lowest energy (Hudson *et al.*, 1982). Since these symmetry designations apply only to the equilibrium nuclear configurations of the molecules and there are many degrees of freedom, it follows that no electronic transitions are strictly forbidden: the zero-point motion can always allow the nuclei to seek out a configuration that is sufficiently distorted for the transition to become allowed. The magnitude of this so-called Herzberg–Teller contribution to the absorption coefficient depends on a variety of factors, including the proximity of intense electronic transitions for molecules having the equilibrium structure. Typically, for aromatics the extinction coefficient ε_{max} of such induced spectra is ~ 500 liters mol^{-1} cm^{-1} (absorption cross section σ of $\sim 2 \times 10^{-18}$ cm^2), whereas the allowed parts, when they occur, have $\varepsilon_{max} \approx 10^4$ liters mol^{-1} cm^{-1} ($\sigma \approx 4 \times 10^{-17}$ cm^2). While the allowed $\pi \rightarrow \pi^*$ transitions of aromatics and polyenes are relatively strong, the symmetry-allowed $n \rightarrow \pi^*$ transitions, because of the small overlap of the electronic orbitals involved, are often 10–100 times less intense. Also intense are some transitions where the charge is substantially displaced in the excited state. These include many polar dyes, where the optical transition approximately corresponds to a transformation into a quinoidal

structure, and conjugated systems having separated electron donor (such as dimethylamine) and acceptor (such as nitro) substituents. Another example of very strong transitions occurs for weak charge-transfer complexes (Mulliken charge transfer), where an electron is transferred completely from the donor to the acceptor on excitation (Mulliken and Person, 1975). While such materials are not as useful in applications where transparency is required, they are excellent candidates for the exploration of resonant nonlinear processes.

The difference between the ground- and excited-state dipole moments $\Delta\mu$ in these cases that involve substantial electron transfer can be extremely large—20 D is not uncommon (Liptay, 1974)—so that this contribution to the magnitude of the nonlinear response can be dominant. The excited-state dipole moments are readily measured in solids by studies of spectra in electric fields (Hochstrasser, 1973). Moderately large values of $\Delta\mu$ of ~ 3 D are found for $n \rightarrow \pi^*$ transitions in heteroaromatics and ketones, but $\Delta\mu \approx 0$ for aromatics even if they are in principle polar.

Besides transitions from the ground states, the spectra of excited organic molecules have also been studied. These transitions are very important to the nonlinear response, since they correspond to the intermediate steps, which occur as either real or virtual transitions, in the multiphoton processes. However, there does not exist such a large data set for excited-state transitions, and there is still a strong reliance on theoretical calculations to predict this important information. Experiments have exposed a few empirical rules that are useful. The excited-state absorption spectra of aromatic molecules resemble the spectra of the corresponding negative ions that have strong absorption in the visible and near ultraviolet. The $n\pi^*$ states have strong absorption bands at low energy, corresponding to changes in the π-electron distribution. Similarly, charge-transfer states have strong transitions to higher-energy neutral states and excited states of the negative and positive ion components. Members of still another class of molecules, the polyphenyls, have excited states with dye-like absorption spectra as a result of the greatly increased conjugation and tendency toward a planar configuration in the excited state compared with the normally nonplanar ground states.

B. Crystal Spectra—Excitons

The electronic and vibrational spectra of molecules are changed on passing to the solid phase. Molecular solids normally contain two or more molecules in each unit cell, so that the crystals consist of two or more interpenetrating lattices. Most neutral molecules form either van der Waals lattices or in addition may form networks through weak chemical interactions such as

hydrogen bonds. Since there is very little electron exchange between the molecules in the structure, the electronic properties of most molecular crystals are adequately described as slightly perturbed versions of the molecular properties. There are of course exceptions to this, including the charge-transfer salts, but this chapter will mainly refer to van der Waals or hydrogen-bonded solids.

The molecular excitations can transfer within the crystal, giving rise to excitation bands (Frenkel excitons) of width β. The excitation transfer time is on the order of $\hbar/\beta$, and for many of the most common crystals this time is long compared with the internal vibration periods of the molecules. In this case the Frenkel excitons correspond to the excitations of a slightly perturbed array of approximately harmonic oscillators. Each molecular electronic–vibrational excitation then has its own distinct exciton band. For the ground electronic state, the excitations are usually termed vibrons and β is typically 1–20 cm^{-1}, dependent on whether the vibrational motion corresponds to an oscillating polarizability or an oscillating dipole, the former being Raman-active and the latter for infrared-active (IR-active) modes. The IR-active modes show the largest vibron bandwidths. For electronically excited states, the exciton bands are formed by the electronic interaction, and the transfer of the vibrational energy alone represents a minor perturbation. The bandwidths are then determined by apportioning the electronic interaction in accordance with the Franck–Condon factor of the transition from the ground state to the level in question. In certain cases of very strong optical transitions, the electronic interaction is sufficiently large that new surfaces for nuclear motion are formed in the crystal! That is the so-called strong coupling case, for which it is no longer appropriate to consider the vibrational motion as slow compared with energy transfer. Only weak coupling occurs for molecular ground states and for the excited states of most simple molecular solids consisting of aromatics and their substituted derivatives. The weak coupling also applies when the excited-state equilibrium geometry differs significantly from the ground state, such as for weak charge-transfer complexes.

The energies of transitions to molecular excited states in crystals (Davydov, 1971) for the weak coupling case are given by

$$\Delta E = \Delta\varepsilon + D + \beta(k) \tag{1}$$

where $\Delta\varepsilon$ is the gas-phase transition energy and D is the gas-to-crystal shift resulting from intermolecular interactions that do not involve exchanging the relevant excitation. The exciton band term $\beta(k)$ describes the energy as a function of the wave vector for the relevant excitation. For nearest-neighbor interactions (Robinson, 1970) and a so-called restricted Frenkel limit in which

certain small terms are excluded, $\beta(k)$ for a crystal having two molecules per unit cell has the form

$$\beta(k) = \sum_a 2\beta_{aa}\cos(k_a a) \pm \sum_{a<b} 4\beta_{ab}\cos\left(\frac{k_a a}{2}\right)\cos\left(\frac{k_b b}{2}\right) \tag{2}$$

where β_{ij} (with $i, j = a, b, c$) is the matrix element for transfer between the two sublattices and β_{aa} is the nearest-neighbor transfer along the a chain, and so on. The optical selection rule is $\Delta k \approx 0$ so that spectra show a splitting of the molecular transitions (Davydov splitting), which depends on the number of molecules in the unit cell. These $k \approx 0$ states form a basis for irreducible representations of the factor group of the equilibrium lattice space group, so that symmetry designations are extremely useful in describing the spectroscopic transitions and selection rules.

C. Impurity Spectra

Both chemical and isotopic impurities are readily dissolved in molecular solids to form substitutional solid solutions. Such impurities alter the optical properties through a variety of mechanisms. Most importantly, the band structures are perturbed, resulting in qualitative changes in the exciton dynamics. The optical spectra of the impurities resemble those of the free molecules. For example, the isotopic impurities have transition energies

$$\Delta E = \Delta\varepsilon + D \tag{3}$$

The selection rules for the impurity spectra are determined by the symmetry of the crystal site at which the molecule is located. It is usual that the lineshapes of impurity optical transitions contain both homogeneous and inhomogeneous contributions. The inhomogeneous contributions are most evident at low temperatures, where the limiting widths of optical transitions are in the range of a few reciprocal centimeters. Hole-burning and photon-echo experiments have proven the character of these low-temperature lines (de Vries and Wiersma, 1976; Small, 1983; Hesselink and Wiersma, 1983) but little was yet learned about the origin or specific properties of the inhomogeneties. The homogeneous contributions to the linewidths involve both pure dephasing and population relaxation contributions, which are quite system-dependent. At low temperatures the pure dephasing is induced by local lattice excitations causing fluctuations at the impurity center, whereas the T_1 relaxations are often approximately independent of temperature.

D. Inhomogeneous Broadening—Line Shapes

The exact nature of the strain disorder in molecular crystals is not understood. It has been suggested that the strain field arises from extended dislocations produced during the freezing process. The spectrum of such disorder must be characterized by both a strength and a correlation length. Simple theoretical models have been proposed to account for dephasing due to this kind of disorder. Klafter and Jortner (1977, 1978) derived an approximate lineshape theory for the absorption spectrum of triplet excitons (Hochstrasser, 1976). Abram and Hochstrasser (1980) have treated directly the time evolution of vibron coherence. Both of these theories use a simple tight-binding Hamiltonian to which a site diagonal perturbation is added to describe the effect of the crystal strain field on the site energies. The pure crystal exciton (vibron) band is characterized by a width W. The site energy perturbations are taken to be Gaussian random variables with a correlation length equal to the lattice spacing, and mean squared value σ:

$$\langle \Delta_i \Delta_j \rangle = \delta_{ij} \sigma^2 \tag{4}$$

These theories predict that

(1) When $\sigma > W$, the band is inhomogeneously broadened.
(2) When $\sigma \ll W$, the linewidth is much narrower than σ.
(3) When $\sigma \ll W$ and the $k = 0$ state lies near a band singularity, the lineshape is asymmetric and the corresponding coherence decay is strictly nonexponential.

The magnitude of σ can be evaluated from the lineshape of a dilute isotopic impurity in the host material, assuming that the lineshape is not dominated by lifetime broadening, and that the impurity level is sufficiently separated from the host bands. This point is related to point (1) above in that dilute impurities form a (random) sublattice with vanishing exciton interaction, hence, $W \approx 0$. Point (2) was first layed out theoretically by the calculations of Klafter and Jortner (1978). An explicit discussion of this "motional narrowing" effect was given by Abram and Hochstrasser (1979), who pointed out that the overall coherence loss could be viewed as a competition between the site diagonal disorder and the correlation forced on the site amplitudes by intermolecular (excitonic) coupling. The term σ is the upper bound to the linewidth in the weak disorder model, and the introduction of exchange coupling makes the linewidth smaller. It was then suggested (DeCola *et al.*, 1980b) that the existence of motional narrowing in molecular crystals makes it possible for lifetime broadening to dominate the linewidth of the vibrational transitions even when the intrinsic disorder width is much larger than the population

decay rate. The T_1 processes are also predicted to be influenced by the disorder (Velsko and Hochstrasser, 1985a,b).

E. Relaxation Processes

The nuclear dynamics of molecular solids can be conceptualized by considering the internal and external motions to be separate. With the exception of very-low-frequency vibrations, the internal modes of aromatic crystals might contain very little external motional character. The relaxation processes can then be understood, in a first approximation, by weak coupling of harmonic oscillators. The expectation exists, and this was confirmed theoretically in a few cases (Righini *et al.*, 1983), that the relaxation pathways can be understood by considering the low-order derivatives of the intermolecular potential. Processes involving one lattice mode are expected to dominate. The lattice frequencies extend to ~ 200 cm^{-1} so that these one-phonon anharmonic effects should be dominated by the third-order mixed mode term $\gamma_3 = (\partial^3 V/\partial Q_1, \partial Q_2\, \partial q)_0$ where Q_1 and Q_2 are internal modes and q involves the relative motion of molecules. The relaxation time τ is then given by a Golden rule for each energetically allowed pathway. It is evident that the relaxation of ground-state vibrational levels then corresponds to motion in a set of coupled exciton bands, with the band from one internal mode acting as the trap for vibrational energy in other modes. The dynamics of vibrations in excited electronic states is more complex, since in addition the vibrational and electronic energy can separate with the difference being absorbed or emitted by the external phonons, depending on the temperature (Hochstrasser *et al.*, 1979).

III. BASIC THEORY

A. Introduction

The various ways that molecular systems can interact with optical radiation fields can be classified into the two main categories of dissipative and parametric processes. Dissipative processes exchange energy between the molecules and the light field through absorption and emission. In parametric processes the quantum state of the system is not changed, but energy and momentum are exchanged between different modes of the light field. This conservation of energy and momentum within the field components implies that the interaction of light beams having well-defined frequencies and directions will lead to new beams with new frequencies travelling again in well-

defined directions. To use a chemical analogy, in parametric processes the molecules assume the role of catalysts.

There are two limiting methods by which nonlinear optical experiments are usually performed. In the frequency-domain approach, the response of the molecular system under investigation is measured as a function of the frequencies of the applied laser fields. The result is a spectrum consisting of resonance lines with certain center frequencies, amplitudes, and widths. In the alternative time-domain methods, the frequencies of the lasers are fixed, and the time delay between the very short laser pulses having wide-frequency bandwidths is varied. The resulting decay curves measure directly the relaxation processes in the molecule. For frequency-domain experiments, monochromatic waves provide information about all the system relaxations, whereas for time-domain experiments the ideal light pulses must impact on the system faster than all relaxation processes for the same goal to be achieved. Real laser sources have finite widths both in frequency and in time. In resonant nonlinear processes—which all spectroscopic arrangements are by definition—the choice of "ideal sources" for frequency-domain experiments depends on the complexities of the damping of the coupled levels. The choice of laser pulse width in relation to the damping rates selects a particular timescale, which determines the effective susceptibility of the system. Obviously, slow processes do not contribute to changes occuring during short light pulses.

B. Nonlinear Polarization, Response Function, and Susceptibility

The key quantity for the understanding of both parametric and dissipative processes is the polarization $\mathbf{P}(\mathbf{r}, t)$ induced in the sample by the electric field $\mathbf{E}(\mathbf{r}, t)$ of the light beams. Although nonlinear optical experiments require laser beams with high powers, the interaction energy is often still small enough compared with intramolecular energies to allow a treatment of the problem with perturbation theory even when the molecules are excited on resonance (see, however, Section III.H). This in turn allows a Taylor-series expansion of the induced polarization:

$$\mathbf{P}(\mathbf{r}, t) = \mathbf{P}^{(1)}(\mathbf{r}, t) + \mathbf{P}^{(2)}(\mathbf{r}, t) + \mathbf{P}^{(3)}(\mathbf{r}, t) + \cdots \tag{5}$$

Here we are concerned with the second and third term of this expansion. The first term describes linear absorption, light emission, refraction, and reflection. The second term refers to coherent sum and difference frequency generation. There are no dissipative processes associated with even-order nonlinear polarizations, except when one of the applied fields is a dc field. The third term

is the source of two-photon absorption, Raman scattering, and a variety of coherent spectroscopies like CARS, CSRS, coherent Rayleigh scattering, polarization spectroscopy, phase conjugation, and most pump-probe spectroscopic methods.

In molecules and molecular crystals, the interaction with the laser field can be regarded as local in space, although nonlocal in time. This means that the polarization $\mathbf{P}(\mathbf{r}, t)$ induced at a certain point in space and time depends on the electric field strength $\mathbf{E}(\mathbf{r}, t')$ at that same point in space at all times $t' \leqslant$ time t. In a general way this relation is expressed as a convolution with a molecular response function $R^{(n)}$ (Butcher, 1965):

$$P_i^{(n)}(t) = \int_{-\infty}^{+} \int_{-\infty}^{+} \cdots \int_{-\infty}^{+} dt_1\, dt_2 \cdots dt_n\, R_{ijk\cdots l}^{(n)}(t - t_1, t - t_2, \ldots, t - t_n \times E_j(t_1) E_k(t_2) \cdots E_l(t_n) \tag{6}$$

The response function $R^{(n)}$ is a tensor of rank $n + 1$, and the indices $ijkl$ refer to cartesian coordinates, with summation implied for doubly occuring indices. A physically meaningful response function must be real and vanish for any time argument approaching the remote past. This latter fact means that the molecules have a finite memory. The term $\mathbf{E}(t)$ is the total electric field interacting with the sample and can consist of a series of pulses centered at different times. Then the product EEE in $P^{(3)}$ contains several expressions each related to a particular pulse sequence of up to three pulses.

The ideal light pulses for time-domain spectroscopy have pulse envelopes much shorter than the characteristic time constants of the response function. If we model them by delta functions,

$$\mathbf{E}(t) = \sum_n \mathbf{E}_n = \sum_n \mathscr{E}_n e^{i\omega_n t}\, \delta(t - \tau_n) \tag{7}$$

then the contribution to the polarization $\mathbf{P}^{(3)}$ resulting from the δ-pulse sequence $E_1 E_2^* E_3$ $(\tau_1 < \tau_2 < \tau_3)$ is

$$\mathbf{P}^{(3)}(t) = R^{(3)}(t - \tau_1, t - \tau_2, t - \tau_3) \vdots \mathscr{E}_1 \mathscr{E}_2^* \mathscr{E}_3 \exp(i\omega_1 \tau_1 - i\omega_2 \tau_2 + i\omega_3 \tau_3) \tag{8}$$

The natural description for frequency domain experiments is to express the electric field in terms of its Fourier transform $\mathbf{E}(\omega)$, yielding, for example, the third-order polarization

$$P_i^{(3)}(t) = \int_{-\infty}^{\infty} \int_{-\infty}^{\infty} \int_{-\infty}^{\infty} d\omega_1\, d\omega_2\, d\omega_3\, \chi_{ijkl}(\omega_1, \omega_2, \omega_3) \times E_j(\omega_1) E_k(\omega_2) E_l(\omega_3) \exp[-i(\omega_1 + \omega_2 + \omega_3)t] \tag{9}$$

The nth-order susceptibilities $\chi^{(n)}$ are the Fourier transforms of the molecular response functions:

$$\chi^{(n)}(\omega_1 \cdots \omega_n) = \int_{-\infty}^{\infty} \cdots \int_{-\infty}^{\infty} dt_1 \cdots dt_n R^{(n)}(t_1 \cdots t_n) \exp\left(-i \sum_{j=1}^{n} \omega_j t_j\right) \quad (10)$$

In practice, the applied laser field consists of one or several pulses, each characterized by a pulse envelope in space and time, a mean frequency, and a propagation direction:

$$\mathbf{E}(\mathbf{r}, t) = \sum_j \tfrac{1}{2} \mathscr{E}(j; \mathbf{r}, t) \exp\{i(\omega_j t - \mathbf{k}_j \mathbf{r})\} + \text{c.c.} \quad (11)$$

The envelopes $\mathscr{E}(j; \mathbf{r}, t)$ often vary slowly in time on the scale of an optical period and the relevant molecular dynamics. Then the field is quasi-monochromatic,

$$\mathbf{E}(\mathbf{r}, \omega) = \sum_j \tfrac{1}{2} \{\mathscr{E}(j)\, \delta(\omega + \omega_j) e^{-i\mathbf{k}_j \mathbf{r}} + \mathscr{E}^*(j)\, \delta(\omega - \omega_j) e^{i\mathbf{k}_j \mathbf{r}}\} \quad (12)$$

and the convolution in Eq. (9), for example, reduces to sums of terms each corresponding to the interaction of three Fourier components of the field, such as

$$P_i^{(3)}(\mathbf{r}, t) = \chi_{ijkl}^{(3)}(\omega_1, -\omega_2, \omega_3) \mathscr{E}_j(1; \mathbf{r}, t) \mathscr{E}_k^*(2; \mathbf{r}, t) \mathscr{E}_l(3; \mathbf{r}, t) \times \exp[i(\omega_1 - \omega_2 + \omega_3)t - i(\mathbf{k}_1 - \mathbf{k}_2 + \mathbf{k}_3) \cdot \mathbf{r}] \quad (13)$$

This polarization again has the form of a plane wave, with the frequency and wave vector the sum of the frequencies and wave vectors of the interacting field components. The sign of each contribution in these sums is positive for each $\mathscr{E}(j)$ and negative for each $\mathscr{E}^*(j)$. Thus knowledge of the product $\mathscr{E}(1)\mathscr{E}^*(2)\mathscr{E}(3)$ completely determines the whole expression of Eq. (13).

C. Nonlinear Dissipative Processes

The energy exchanged between the light beam and the molecular ensemble, per unit time and volume, is given by

$$\frac{dW}{dt} = \langle \mathbf{E} \cdot \dot{\mathbf{P}} \rangle \quad (14)$$

where the brackets indicate a time average over several cycles of the electric field. For monochromatic waves with amplitudes $\mathscr{E}$ and $\mathscr{P}$ and the same frequency ω, this average is

$$\frac{dW}{dt} = \tfrac{1}{2} \omega \text{Im}(\mathscr{E} \cdot \mathscr{P}) \quad (15)$$

As an example we consider two-photon absorption. The relevant nonlinear polarization at frequency ω is

$$\tfrac{1}{2}\mathscr{P}\exp(i\omega t) = \tfrac{1}{8}\chi^{(3)}(-\omega,\omega,\omega)\vdots\mathscr{E}\mathscr{E}\mathscr{E}^*\exp(i\omega t) \tag{16}$$

The energy absorbed through two-photon processes is therefore

$$\frac{dW}{dt} = \frac{8\pi^2\omega}{n^2c^2}I^2\mathrm{Im}(\chi^{(3)}) \tag{17}$$

where we have used $I = \mathscr{E}\mathscr{E}^*nc/8\pi$ for the intensity of the laser beam. In a rate equation description, two-photon absorption is often described through a cross section δ in units of cm^4 sec as

$$dn_p/dt = \delta NF^2 \tag{18}$$

where dn_p/dt is the number of photons absorbed per unit time, N the density of absorbing molecules, and $F = I/\hbar\omega$ the photon flux (McClain and Harris, 1978). Since $dW = dn_p\hbar\omega$, the relation between the cross section δ and the susceptibility $\chi^{(3)}$ is (Bechtel and Smith, 1976; Burris *et al.*, 1983):

$$\delta = \frac{8\pi^2\hbar\omega^2}{n^2c^2N}\mathrm{Im}(\chi^{(3)}) \tag{19}$$

Equation (19) can be used to measure two-photon cross sections through coherence experiments (Lotem and Lynch, 1976; Lynch and Lotem, 1977; Hochstrasser *et al.*, 1980). A similar relation is valid for Raman cross sections and can be deduced along the same lines (Bloembergen, 1965; Shen, 1974):

$$\frac{d^2\sigma}{d\omega_S d\Omega} = \frac{\hbar\omega_L\omega_S^3}{\pi c^4}\mathrm{Im}[\chi^{(3)}(\omega_L,\omega_S,-\omega_L)] \tag{20}$$

This kind of relation is quite general: all cross sections for absorption and stimulated emission can be related to the imaginary part of a susceptibility. Even the spontaneous emission can be obtained from this classical description when the black-body radiation field is taken as the "stimulating" field.

D. Optics of Parametric Processes

The temporal and spatial evolution of the generated light wave is described by the inhomogeneous Maxwell equations with the nonlinear polarization as source term:

$$\begin{aligned}\nabla\times\nabla\times\mathbf{E} + \frac{\varepsilon(\omega)}{c^2}\left(\frac{\partial^2}{\partial t^2}\right)\mathbf{E} &= -\frac{4\pi}{c^2}\left(\frac{\partial^2}{\partial t^2}\right)\mathbf{P}^{\mathrm{NL}} \\ \nabla\cdot[\varepsilon(\omega)\mathbf{E} + 4\pi\mathbf{P}^{\mathrm{NL}}] &= 0\end{aligned} \tag{21}$$

We treat the complex dielectric tensor $\varepsilon(\omega) = 1 + 4\pi\chi^{(1)}(\omega)$ as a scalar, which is appropriate for isotropic media or beams travelling perpendicular to a principal direction in birefringent crystals. To account for linear absorption, we take the wave vectors of all waves to be complex:

$$\mathbf{K}_j = \hat{\mathbf{e}}_j(k_j - ia_j) \tag{22}$$

In this expression, $\hat{\mathbf{e}}_j$ is a unit vector perpendicular to the travelling wavefront, k_j is the usual wave vector in the medium with length $n\omega/c$, and a_j is half the linear absorption coefficient of the medium at frequency ω_j.

When the polarization wave is not attenuated through nonlinear depletion of the pump waves (i.e., for small conversion efficiencies), integration of Maxwell's equation with the slowly varying envelope method (Bloembergen, 1965; Butcher, 1965) yields for the amplitude of the generated wave

$$\mathscr{E}(L, t_R) = \frac{2\pi\omega^2}{c^2 K_S}\mathscr{P}(t_R) \cdot \frac{\exp(i\Delta KL) - 1}{\Delta K} \tag{23}$$

In this expression L is the interaction length, $\Delta K = K_s - K_p$ is the phase mismatch, and K_s and K_p are the complex wave vectors of the signal and the polarization wave, respectively. The time argument t_R is a reduced time,

$$t_R = t - \mathbf{k}_S \cdot \mathbf{r}/\omega \tag{24}$$

which serves to effectively transform into a rest frame for the light pulses in time-domain processes. The instantaneous intensity of the generated light beam after an interaction length L is

$$\begin{aligned} I_S(L, t_R) &= \frac{cn_S}{8\pi}|\mathscr{E}(L, t_R)\exp[i(\omega t - \mathbf{k}_S\mathbf{r})]|^2 \\ &= \frac{n_S\pi\omega^4}{2c^3(k_S^2 + a_S^2)} \cdot |\mathscr{P}^{NL}(t_R)|^2 \cdot G(L) \end{aligned} \tag{25}$$

Usually the signal is not resolved in time, but the integral is measured:

$$I_S(L) = \frac{n_S\pi\omega^4}{2c^3(k_s^2 + a_s^2)} G(L) \cdot \int_{-\infty}^{+\infty} dt_R |\mathscr{P}^{NL}(t_R)|^2 \tag{26}$$

The phase mismatch and absorption factor

$$G(L) = L^2 \frac{\sinh^2(\Delta aL/2) + \sin^2(\Delta kL/2)}{(\Delta aL/2)^2 + (\Delta kL/2)^2} e^{-(a_s + a_p)L} \tag{27}$$

where $\Delta a = a_s - a_p$, is of particular interest in spectroscopic applications since it contains all information regarding the growth of the signal in propagating through the sample. It is necessary for estimating the optimum

concentrations and interaction lengths. In the absence of absorption, $G(L)$ can increase as L^2. In the presence of absorption, an optimum exists for the interaction length, depending on a_s and a_p. Since a_s and a_p are both proportional to the concentration c of the molecular system, the signal can be optimized for a particular interaction length L through the choice of concentration. The interaction length itself is usually given through the confocal parameters of the beam-combining optics or the size of the sample cuvette. The signal depends on the concentration c through $a_s = \sigma_s c/2$ and $a_p = \sigma_p c/2$, where σ_s and σ_p are the molecular absorption cross sections for the signal and polarization waves. With phase matching, the signal is a function of the product Lc, which has the optimum value

$$(Lc)_{opt} = \frac{2\ln(\sigma_s/\sigma_p)}{\sigma_s - \sigma_p} \tag{28}$$

E. Molecular Theory of the Susceptibilities

To connect the observed macroscopic quantities to the molecular properties of interest, we write the macroscopic polarization as the ensemble average of the induced molecular dipoles,

$$\mathbf{P} = N\langle \boldsymbol{\mu} \rangle \tag{29}$$

where N is the number density of the molecules in the sample. The ensemble average is the trace of the product of the molecular dipole operator with the statistical (or density) operator ρ of the molecule:

$$\langle \boldsymbol{\mu} \rangle = \mathrm{Tr}\{\rho \boldsymbol{\mu}\} \tag{30}$$

The density operator in turn obeys an equation of motion (Liouville equation) of the following form:

$$\dot{\rho} = \frac{i}{\hbar}[\rho, V] + \dot{\rho}^{\mathrm{R}} \tag{31}$$

All operators are in the interaction picture, and the interaction operator $V(t)$ in the dipole approximation is

$$V(t) = -\boldsymbol{\mu}(t) \cdot \mathbf{E}(t) \tag{32}$$

where the matrix elements are $\mu_{ab}(t) = \mu_{ab} \exp(i\omega_{ab} t)$, $\omega_{ab} = (\varepsilon_a - \varepsilon_b)/\hbar$, and ε_i are the level energies of the molecule. The last term $\dot{\rho}^{\mathrm{R}}$ in Eq. (31) is a phenomenological damping term accounting for the relaxation of the molecular excitations. Its particular form depends on the model for the partitioning of the molecular system into relevant states and bath states. In the

Markov approximation limit the decay is assumed to be exponential, and the matrix elements of $\dot{\rho}^{R}$ are

$$\dot{\rho}^{R}_{\mu\mu} = -\Gamma_{\mu\mu}\rho_{\mu\mu} + \sum_{\nu \neq \mu} \gamma_{\nu\mu}\rho_{\nu\nu} \tag{33}$$

$$\dot{\rho}^{R}_{\mu\nu} = -\Gamma_{\mu\nu}\rho_{\mu\nu} \tag{34}$$

Equation (33) describes the decay of the populations (diagonal elements of ρ) with rate constants $\Gamma_{\mu\mu}$ (inverse lifetimes T_1), as well as the feeding through the decay of other levels ν to the level μ with rate constants $\gamma_{\nu\mu}$. Equation (34) accounts for the decay of the off-diagonal elements (coherence loss) with the phase-relaxation rate $\Gamma_{\mu\nu} = 1/T_2(\mu\nu)$. This phase-relaxation rate is the mean of the population decay rates of the two levels plus a pure dephasing rate $\Gamma'_{\mu\nu}$:

$$\Gamma_{\mu\nu} = \tfrac{1}{2}(\Gamma_{\mu\mu} + \Gamma_{\nu\nu}) + \Gamma'_{\mu\nu} \tag{35}$$

The system and the bath are often chosen such that the latter vanishes under collision-free conditions, and in solids for low temperatures ($T \to 0$).

The system of coupled linear differential equations [Eq. (31)] can be decoupled in two steps. First the statistical operator is expanded in a Taylor series in powers of the interaction (i.e., electric field strength) by analogy to the expansion of the polarization:

$$\rho = \rho^{(0)} + \rho^{(1)} + \rho^{(2)} + \rho^{(3)} + \cdots \tag{36}$$

The second step is the neglect of the feeding constants $\gamma_{\nu\mu}$. This can be justified *a posteriori* when the perturbation theory expression for a particular matrix element of interest involves no excited-state populations, which is true in many important examples. The decoupled equations can then be integrated to yield (in the following we set $\hbar = 1$)

$$\rho^{(n+1)}_{\mu\nu} = ie^{-\Gamma_{\mu\nu}t} \int_{-\infty}^{t} dt' \, e^{\Gamma_{\mu\nu}t'} [\rho^{(n)}(t'), V(t')]_{\mu\nu} \tag{37}$$

The density matrix can now be iteratively calculated to any desired order. When the perturbation is a monochromatic wave in each step, the density matrix in each order will decompose into a sum of Fourier components at all combination frequencies of the ingoing fields. After taking the trace with the molecular dipole operator, the susceptibilities are recognized as the various Fourier coefficients:

$$\mathrm{Tr}\{\rho^{(n)}\boldsymbol{\mu}\} = \chi^{(n)} \cdot \mathbf{E}^{n} \tag{38}$$

There are, however, many time orderings and different pathways that contribute to the same Fourier component. For example, a Fourier component at frequency $\omega_4 = \omega_1 - \omega_2 + \omega_3$ is generated in third order by perturbations with the field components $\mathscr{E}_1$, $\mathscr{E}_2^*$, and $\mathscr{E}_3$ considered in $V(t)$, for

which six different time orderings are possible. Furthermore, the interaction can be through the part ρV or the part $-V\rho$ of the commutator $[\rho, V]$ in Eq. (37). This is sometimes called evolution of the bra part or the ket part of the density operator. The interference between all these contributions often plays an important role in steady-state experiments, and diagrammatic methods have been developed to find all important terms (Bordé, 1976; Bordé and Bordé, 1978; Yee *et al.*, 1977; Yee and Gustafson, 1978; Druet *et al.*, 1978; Oudar and Shen, 1980). A method that is especially useful when molecular resonances are considered is shown in Fig. 1 (Dick and Hochstrasser, 1983a; Bozio *et al.*, 1983).

The figure shows the evolution of a particular diagram from left to right. The broken and full vertical arrows represent evolution of the ket and bra parts, respectively, in time ordering from left to right. The numbers at the bottom of the diagram below each arrow indicate the frequency of the field

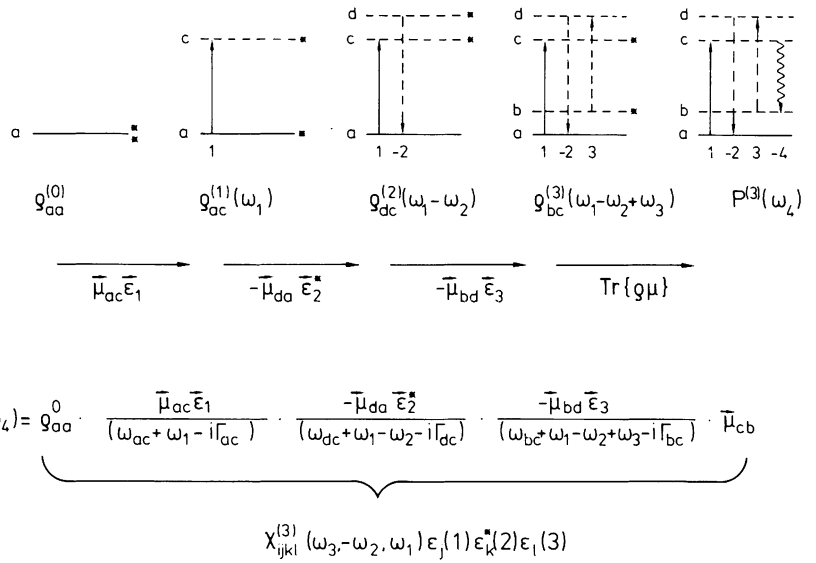

Fig. 1. Diagrammatic method for the calculation of nonlinear susceptibilities. As an example, a contribution to $\chi^{(3)}(\omega_3, -\omega_2, \omega_1)$ through a CSRS effect is shown. The development of the diagram through the orders of perturbation theory proceeds from left to right, the rightmost diagram being the final result. Each iteration adds a full or broken arrow to the diagram, representing evolution of the bra or the ket side of the density operator. The head of the latest full arrow and the tail of the latest broken arrow determine the indices of the current matrix element of the density operator. These are given in the second row in the figure, and the corresponding levels are marked by asterisks in the diagram. The third row gives the perturbation considered in each step coupling the connected levels. A minus sign indicates evolution of the ket (corresponding to a broken arrow in the diagram), and asterisk denotes the negative frequency component of the field (corresponding to a downward arrow). The formula represented by the diagram is given, where the five factors from left to right correspond to the five steps in building the diagram.

component. The arrow points upward when the positive frequency (i.e., photon creation) is involved, and downward if it is the negative frequency (i.e., the complex conjugate wave). The first arrow of each type starts from the level labeled "a," which represents the initial state. The full arrows point in the sense of the transition, whereas the broken arrows go in the opposite sense.

The corresponding mathematical expression starts with the population of the initial state, here $\rho_{aa}^{(0)}$. Each step in the perturbation expansion contributes a factor whose numerator is the coupling matrix element, and whose denominator is

$$\omega_{\mu\nu} + \sum_j \omega_j - i\Gamma_{\mu\nu} \tag{39}$$

Here $(\mu\nu)$ is the index pair of the density matrix element being calculated (marked with the asterisk), and the sum is over all frequencies involved in the process up to this point. The last dipole factor comes from the trace operation and corresponds to the curly arrow that closes the loop and represents the generated wave.

The same diagrammatic technique can be applied to obtain the response functions, by using delta-function pulses, as in Eq. (7), in the iterative calculation of the density matrix [Eq. (37)]. After taking the trace $\mathrm{Tr}(\rho\boldsymbol{\mu})$, the molecular expression for the polarization is of the form of Eq. (8), and the response function is easily identified. By analogy with the susceptibilities, a recipe can be given to obtain the response function directly from the corresponding diagram. The first term is again the population of the initial state, $\rho_{aa}^{(0)}$. Each iteration yields a factor

$$-i\mu_{xy}\exp[+(i\omega_{\mu'\nu'} + \Gamma_{\mu'\nu'})t_n - (i\omega_{\mu\nu} + \Gamma_{\mu\nu})t_n] \tag{40}$$

Here (xy) is the index pair of the transition dipole matrix element involved in the interaction with the field ε_n at time τ_n and $t_n = t - \tau_n$. The index pair $(\mu\nu)$ is the one of the required density matrix element, whereas the index pair $(\mu'\nu')$ refers to the density matrix element of the previous iteration step. The last factor is again the transition dipole element from the trace operation. For the diagram developed in Fig. 1, the response function is

$$\begin{aligned} R^{(3)}(t_1, t_2, t_3) = &-i\rho_{aa}^{(0)}\mu_{ac}\mu_{da}\mu_{bd}\mu_{cb} \\ &\times \exp\{-[(i\omega_{ac} + \Gamma_{ac})(t_1 - t_2) \\ &+ (i\omega_{dc} + \Gamma_{dc})(t_2 - t_3) + i\omega_{bc} + \Gamma_{bc})t_3]\} \end{aligned} \tag{41}$$

To obtain the correct susceptibility from the response function of Eq. (41), the Fourier transform must be performed with $\exp[i(\omega_1 t_1 - \omega_2 t_2 + \omega_3 t_3)]$.

The horizontal broken lines in Fig. 1 really refer to the complete set of eigenstates of the molecule, or virtual states having the photon energy, and the

correct expression for the contribution to the susceptibility or the response function must be summed over all indices. It is clear that many different time orderings and combinations of bra and ket evolutions will contribute to the same Fourier component of ρ, but only a few diagrams have important contributions when resonances are considered.

As an example we discuss sum frequency mixing with two ingoing frequencies. The relevant Fourier component of ρ is $\rho^{(2)}(\omega_1 + \omega_2)$. Two time orderings are possible, namely $\mathscr{E}_1\mathscr{E}_2$ and $\mathscr{E}_2\mathscr{E}_1$. In each step the interaction can be on the bra or the ket side, making a total of eight diagrams. These are given in Fig. 2.

For a diagram to give any contribution at all, the starting level, marked by a dot in Fig. 2, must be populated. When this is the ground state of the molecule, all states that can act as intermediate states (broken lines) lie at higher energies. Diagrams involving arrows connecting the ground state with an even lower-lying intermediate state will always be far off-resonant, and can be neglected in the presence of other resonant diagrams. This neglect is mathematically equivalent to making the rotating wave approximation (RWA). It follows that only diagrams 1 and 5 in Fig. 2 need to be considered for a molecule in its

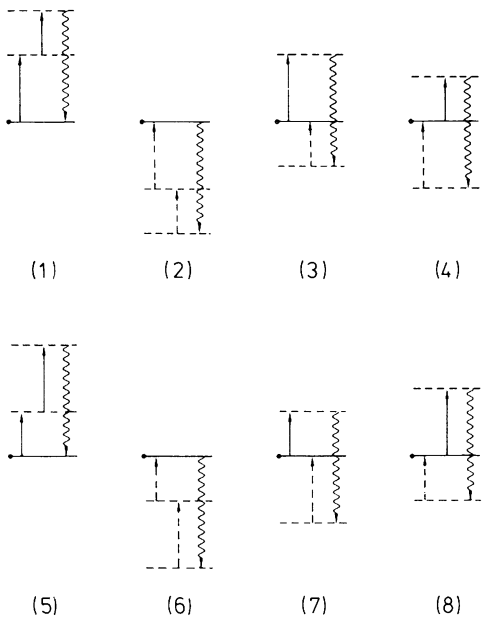

Fig. 2. The eight time-ordered diagrams for sum-frequency generation in second order, representing $P(\omega_1 + \omega_2)$. The initial state is marked by the dot.

ground state. Of course, diagrams like 3 and 4 can become important for processes starting from an excited state.

Extension of the method to third-order processes is straightforward, although the number of possible diagrams increases dramatically. For a Fourier component resulting from the mixing of three different frequencies, six time orderings and 48 diagrams arise. The Fourier component $2\omega_1 - \omega_2$ familiar from CARS (coherent anti-Stokes Raman scattering) still contains 24 diagrams, but 16 of them involve intermediate states below the starting level. The remaining eight are shown in Fig. 3. The introduction of resonance conditions will assign these to different physical processes. With $2\omega_1$ chosen in resonance with a transition $|a\rangle \rightarrow |d\rangle$, only diagrams 1 and 2 will contribute. Although at first glance diagrams 7 and 8 might seem important too, the

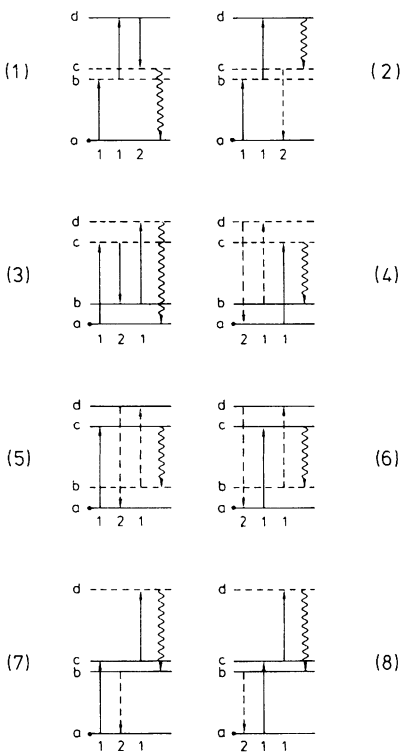

Fig. 3. Eight out of the possible 24 diagrams for $P(2\omega_1 - \omega_2)$. The other 16 diagrams can be neglected due to the rotating-wave approximation for molecules in their ground state (marked by the dot). Molecular resonances, indicated by the full horizontal lines at the energies of real states, allow these diagrams to be assigned to various spectroscopies: (1, 2) two-photon spectroscopy; (3) CARS of a ground-state Raman transition; (4) CSRS of a ground-state Raman transition; (5, 6) CSRS of an excited-state Raman transition; (7, 8) CARS of an excited-state Raman transition.

corresponding $\chi^{(3)}$ shows no resonance denominator related to the two-photon resonance. This is because the path through the perturbation theory never leads to a coherence ρ_{ad} for these diagrams. [The paths are $\rho_{ac}^{(1)}$ to $\rho_{bc}^{(2)}$ to $\rho_{bd}^{(3)}$ and $\rho_{ba}^{(1)}$ to $\rho_{bc}^{(2)}$ to $\rho_{bd}^{(3)}$]. Of particular interest besides two-photon resonances are Raman resonances in ground and excited states. Ground-state Raman resonances are contained in diagram 3 for $\omega_1 > \omega_2$ and diagram 4 for $\omega_1 < \omega_2$. These are the classical CARS and CSRS (coherent Stokes Raman scattering). The excited-state Raman resonances require that the ingoing frequencies are also each resonant with a one-photon transition. For the CSRS configuration (diagrams 5 and 6), a molecular vibrational level will always lie close to the position for the intermediate level $|b\rangle$, making these diagrams in effect fully resonant. Interference between these two diagrams results in the extra resonances.

F. Discussion of Examples

The susceptibilities can be classified according to the number of resonances. This can lead to considerable simplification of the mathematical expressions. As an example we take the CARS susceptibility for a molecule in its ground state in the rotating-wave approximation (diagram 3 of Fig. 3):

$$\chi_{\mathrm{CARS}}^{(3)} = \sum_{b,c,d} \frac{\mu_{ac}\mu_{cb}\mu_{bd}\mu_{da}}{(\omega_{ac} + \omega_1 - i\Gamma_{ac})(\omega_{ab} + \omega_1 - \omega_2 - i\Gamma_{ab})(\omega_{ad} + 2\omega_1 - \omega_2 - i\Gamma_{ad})} \tag{42}$$

When ω_1 and ω_2 are both far from any electronic resonance of the molecule, only the second denominator will lead to resonances for those states $|b\rangle$ for which $\omega_{ab} + \omega_1 - \omega_2 = 0$ in the range over which ω_1 and ω_2 are scanned in the experiment. In this case we can write

$$\chi_{\mathrm{CARS}}^{(3)} = \sum_{b}{}' \frac{R_{ab}}{\omega_{ab} + \omega_1 - \omega_2 - i\Gamma_{ab}} + \chi_{\mathrm{NR}}^{(3)} \tag{43}$$

The prime at the summation symbol indicates that the sum is only over resonant states $|b\rangle$. All other terms are incorporated in the nonresonant susceptibility $\chi_{\mathrm{NR}}^{(3)}$, which is often constant in the frequency range of interest. The amplitudes R_{ab} are related to the Raman transition polarizabilities $\alpha(\omega)$:

$$\begin{aligned} R_{ab} &= \alpha_{ab}(\omega_1)\alpha_{ba}(2\omega_1 - \omega_2) \\ \alpha_{ab}(\omega) &= \sum_{c} \frac{\mu_{ac}\mu_{cb}}{\omega_{ac} + \omega - i\Gamma_{ac}} \end{aligned} \tag{44}$$

The damping parameters Γ can be neglected in all nonresonant denominators, making χ_{NR} and the Raman amplitudes real. Other single resonant sus-

ceptibilities can be contracted in the same way. For example, the two-photon resonant susceptibility resulting from the diagrams 1 and 2 of Fig. 3 can be written as

$$\chi^{(3)}_{\mathrm{TPA}} = \sum_d{}' \frac{T_{ad}}{\omega_{ad} + 2\omega_1 - i\Gamma_{ad}} + \chi^{(3)}_{\mathrm{NR}}$$
$$T_{ad} = \alpha_{ad}(\omega_1)[\alpha_{da}(\omega_2) + \alpha_{da}(2\omega_1 - \omega_2)] \tag{45}$$

Difference-frequency generation is an example of a doubly resonant process. The two relevant diagrams are shown in Fig. 4. With the method outlined above, we obtain for the resonant part of the response functions

$$R_1(t_2, t_1) = -\mu_{ac}\mu_{ba}\mu_{cb}\exp[-(i\omega_{ac} + \Gamma_{ac})(t_2 - t_1) - (i\omega_{bc} + \Gamma_{bc})t_1] \tag{46}$$

$$R_2(t_1, t_2) = -\mu_{ba}\mu_{ac}\mu_{cb}\exp[-(i\omega_{ba} + \Gamma_{ba})(t_1 - t_2) - (i\omega_{bc} + \Gamma_{bc})t_2] \tag{47}$$

Excitation by very short light pulses yields a nonlinear polarization given by these response functions, and the integrated signal at the detector is

$$I_1 = \int_{\tau_1}^{\infty} |R_1(t - \tau_2, t - \tau_1)|^2\, dt = \frac{\mu_{ba}^2\mu_{ac}^2\mu_{cb}^2}{2\Gamma_{bc}}\exp[-2\Gamma_{ac}(\tau_1 - \tau_2)] \tag{48}$$

$$I_2 = \int_{\tau_2}^{\infty} |R_2(t - \tau_1, t - \tau_2)|^2\, dt = \frac{\mu_{ba}^2\mu_{ac}^2\mu_{cb}^2}{2\Gamma_{bc}}\exp[-2\Gamma_{ab}(\tau_2 - \tau_1)] \tag{49}$$

Different time ordering of the two light pulses will thus measure different relaxation times of the molecule. The susceptibilities corresponding to the two diagrams are

$$\chi_1 = \frac{-\mu_{ac}\mu_{ba}\mu_{cb}}{(\omega_{ac} + \omega_2 - i\Gamma_{ac})(\omega_{bc} + \omega_2 - \omega_1 - i\Gamma_{bc})} \tag{50}$$

$$\chi_2 = \frac{-\mu_{ac}\mu_{ba}\mu_{cb}}{(\omega_{ba} - \omega_1 - i\Gamma_{ab})(\omega_{bc} + \omega_2 - \omega_1 - i\Gamma_{bc})} \tag{51}$$

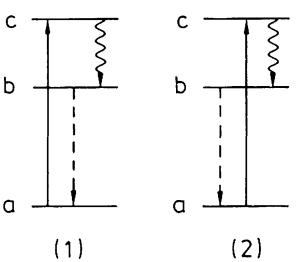

Fig. 4. The two time-ordered diagrams describing difference-frequency generation.

They can be obtained by Fourier-transforming Eqs. (46) and (47), or directly from the diagrams. In a frequency-domain experiment, the time ordering of the interactions cannot be distinguished, and the effective susceptibility is the sum of χ_1 and χ_2:

$$\chi_{\text{eff}} = \chi_1 + \chi_2 = \frac{\mu_{ac}\mu_{ba}\mu_{cb}}{(\omega_{ac} + \omega_2 - i\Gamma_{ac})(\omega_{ab} + \omega_1 + i\Gamma_{ab})} \times \left(1 - i\frac{\Gamma'_{ab} + \Gamma'_{ac} - \Gamma'_{bc}}{\omega_{bc} + \omega_2 - \omega_1 - i\Gamma_{bc}}\right) \tag{52}$$

The result of the interference of both diagrams is the so-called DICE resonance (Andrews and Hochstrasser, 1981a,b; Andrews *et al.*, 1981) appearing in the large parentheses. The numerator of this resonance contains only pure dephasing rates, and thus the amplitude of this resonance is a measure of pure dephasing events.

G. Inhomogeneous Broadening and Line Narrowing

The susceptibilities or response functions calculated up to this point refer to a single molecule or a homogeneous ensemble of noninteracting molecules. In inhomogeneous systems, different sets of molecules have different transition energies, and the total susceptibility is the ensemble average. For a single resonance, the average is

$$\langle\chi\rangle = \int_{-\infty}^{+\infty} dx\, g(x) \frac{A}{\omega_A + x + \omega - i\Gamma} \tag{53}$$

where ω_A is the mean transition frequency of the ensemble, x the frequency shift for a particular molecule, and $g(x)$ the probability distribution function of the inhomogeneous distribution. When the inhomogeneous distribution is the result of a large number of independent perturbations (e.g., due to different environments in a solid), the distribution probability $g(x)$ is Gaussian. This is also the case for the Doppler distribution in gas phase. In this case,

$$g(x) = (2\pi\sigma^2)^{-1/2} \exp(-x^2/2\sigma^2) \tag{54}$$

$$\langle\chi\rangle_\sigma = i(\pi/2)^{1/2}\sigma^{-1}AW\left[\frac{i\Gamma - \omega_A - \omega}{(2\sigma)^{1/2}}\right] \tag{55}$$

where $W(z)$ is the complex error function. Its width is mainly determined by the larger of the two widths Γ and σ, the homogeneous and inhomogeneous widths. The main effect is immediately visible when $g(x)$ is approximated by a

Lorentzian:

$$g(x) = (\sigma/\pi)(\sigma^2 + x^2)^{-1} \tag{56}$$

$$\langle\chi\rangle_L = \frac{A}{\omega_A + \omega - i(\Gamma + \sigma)} \tag{57}$$

The linewidth of the averaged susceptibility is the sum of the homogeneous and the inhomogeneous width. When the inhomogeneous width is dominant, the singly resonant susceptibility cannot be used to obtain homogeneous parameters of the system. In multiply resonant systems, however, the average over broad inhomogeneous distributions can lead to homogeneous resonance lines. To understand these so-called line-narrowing effects, let us consider a doubly resonant susceptibility,

$$\chi(x, y) = \frac{A}{(\omega_a + \omega_1 + x - i\Gamma_1)(\omega_b + \omega_2 + y - i\Gamma_2)} = \frac{A}{(\Omega_a + x)(\Omega_b + y)} \tag{58}$$

where ω_a and ω_b are the center frequencies of the transitions, and x and y the frequency shifts for a particular molecule. The distribution of the frequency shifts for the ensemble of molecules is described by a two-dimensional distribution function $g(x, y)$. When the distributions of x and y are uncorrelated, the distribution function factors into $g(x, y) = g_1(x)g_2(y)$, and the average

$$\langle\chi\rangle = \int\int dx\, dy\, \chi(x, y)g(x, y) \tag{59}$$

breaks up into the product of two terms like Eq. (54), leading to broad inhomogeneous resonances. In the other extreme of complete correlation between the distributions,

$$g(x, y) = \tilde{g}(x)\,\delta(y - \alpha x) \tag{60}$$

the integral reduces to

$$\langle\chi\rangle = \int dx\, \tilde{g}(x) \frac{A}{(\Omega_a + x)(\Omega_b + \alpha x)} \tag{61}$$

When $\tilde{g}(x)$ is approximated by a Lorentzian, Eq. (62) can be solved by contour integration. When α is positive there is only one pole, at $-i\sigma$, lying below the real axis, so that the resulting $\langle\chi\rangle$ is

$$\langle\chi\rangle = \frac{A}{(\Omega_a - i\sigma)(\Omega_b - i\alpha\sigma)} \tag{62}$$

This contains two broad resonances. However, when α is negative, a second term arises and the susceptibility becomes

$$\langle \chi \rangle = \frac{A}{\Omega_b - \alpha\Omega_a} \cdot \left[\frac{1}{\Omega_a - i\sigma} - \frac{\alpha}{\Omega_b + i\alpha\sigma} \right] \quad ; \alpha < 0 \tag{63}$$

The susceptibility now has a resonance denominator with only homogeneous linewidth parameters. The average can also be performed with a gaussian distribution function, and the numerical evaluation of the complex error function shows the same effect (Dick and Hochstrasser, 1983a). Thus, the line-narrowing properties are intimately connected with the correlations within the inhomogeneous lines for each of the transitions involved in the overall process (i.e., each of the resonances).

H. Strong Light Fields

The perturbative description of the interaction between light fields and molecular systems breaks down when very strong light fields are resonant with molecular transitions. Since our interest is in these resonant situations, a careful analysis of the applicability of perturbation theory is in order. For the two-level system, the exact solution of the Liouville equation [Eq. (31)] within the rotating-wave approximation is well known and has been discussed many times. [For a review, see Allen and Eberly (1975) or Schmalz and Flygare (1978).] The exact result is well represented by the perturbation theory expression as long as

$$\Omega = \mu_{12} E/2\hbar \ll (\Gamma_{12}^2 + \Delta^2)^{1/2} \tag{64}$$

where μ_{12} is the transition dipole, E the field amplitude, Γ_{12} the transverse relaxation rate, Δ the detuning from resonance, and Ω the Rabi frequency (Rabi, 1937). For large field strengths that violate Eq. (64), the perturbation theory is no longer applicable. The exact solution describes power broadening, saturation, ac Stark effects, and optical nutation.

Strong field effects are also expected in nonlinear spectroscopic experiments in multilevel systems if one or more of the ingoing laser fields violates Eq. (64) for a particular transition. The simplest case is an N-level system in full resonance with $N - 1$ laser fields. In this case, a unitary transformation will remove all rapidly time-dependent terms (Dick and Hochstrasser, 1983b). In the steady state, a simple linear equation system yields the density operator of the molecular system. The latter can be used to calculate parametric processes (Dick and Hochstrasser, 1983b), as well as stimulated or spontaneous dissipative processes (Dick and Hochstrasser, 1983c, 1984b). Two interesting

new effects are predicted:

1. In parametric processes, a splitting of resonances without power-broadening is possible. For example, in a CARS experiment where the interaction of the pump beam with an electronic transition is strong, the Rabi frequency of this interaction will show up as a splitting of the CARS resonance, whereas the width of the CARS resonance will not be affected. This effect could be used to measure transition dipoles.
2. The extra resonances induced through pure dephasing processes in the framework of perturbation theory will appear as power-induced extra resonances, even in the absence of pure dephasing.

IV. SELECTED EXAMPLES

A. Introduction

Since tunable dye lasers became available over 10 years ago, a great variety of nonlinear spectroscopic techniques has been developed and applied to molecular condensed matter. The first high-resolution two-photon spectra of molecular crystals were obtained by Hochstrasser *et al.* (1973a,b, 1974), who recorded the spectra of benzene, naphthalene, and biphenyl at liquid-helium temperatures by monitoring the ultraviolet (UV) fluorescence of these materials subsequent to two-photon absorption from a pulsed dye laser. The increase of spectroscopic information obtained in these experiments is analogous to the importance of Raman versus infrared for vibrational spectroscopy. In both cases different selection rules make new transitions observable, and six tensor versus three vector components probe in more detail the anistropy of a molecule. A technical advantage is that bulk crystals can be used because the materials are transparent at the incident laser frequency, yet only a small volume is probed, and these experiments are therefore less sensitive to strain, which is produced more readily in the very thin samples necessary for linear absorption experiments.

As lasers developed, more demanding experiments could be performed: coherent transients such as photon echos, optical nutation, and optical free induction decay were observed and used to probe the dynamics of molecular systems at low temperatures (for reviews, see Hesselink and Wiersma, 1983; Burns *et al.*, 1983). In the following we shall discuss experiments in which a new frequency component is produced in a parametric process: three- or four-wave mixing, such as sum- and difference-frequency generation via $\chi^{(2)}$, or CARS and CSRS via $\chi^{(3)}$. The spectroscopic information in these experiments is obtained by monitoring the intensity of the generated beam at the new

frequency component as a function of the frequencies of the incident beams. In addition to the spectroscopic information, these experiments yield precise determinations of the nonresonant nonlinear susceptibilities and thus measure important material constants (nonlinear refractive indices). In molecular solids, four-wave mixing is also the most precise method to evaluate two-photon cross-sections of individual vibronic transitions. In these frequency-domain experiments, information about the dynamics is obtained from an analysis of the lineshape and width. This dynamical information can equally well be obtained in time-domain experiments, where the coherence decay is measured directly by monitoring the intensity of the generated signal as a function of the delay between the laser pulses. These measurements are superior for long coherence decay times or when a narrow level structure can be resolved from the resulting beat pattern of the coherence decay.

The choice of examples given below is necessarily arbitrary and is not intended as an exhaustive review. The examples are arranged according to the number of molecular resonance conditions that are simultaneously fullfilled: the case of no resonances is the focus of most of the other chapters in this book and will not be discussed here.

B. Single Resonances

Singly resonant contributions to the susceptibility are those for which only one resonance condition is nearly fullfilled. These resonant contributions occur when the difference or the sum of the frequencies of two incident fields equals the energy difference of a pair of levels connected by a Raman or a two-photon absorption process, or when the frequencies of either the incident or of the generated fields resonate in a one-photon process. At least one of the two levels coupled by the light field must be populated in order to observe such resonances. A system may have any number of singly resonant contributions and the susceptibility has the general form

$$\chi = \langle \chi_{NR} + \Sigma A_{ab}/(\omega_{ab} + \{\omega_l\} \pm i\Gamma_{ab}) \rangle \tag{65}$$

such as specified in Eqs. (43) and (45) for Raman or two photon resonances. The term $\{\omega_l\}$ stands for each of the combinations of frequencies satisfying $\omega_{ab} + \{\omega_l\} = 0$, such as $\{\omega_l\} = \omega_1 - \omega_2$ for Raman resonances and $\{\omega_l\} = 2\omega_1$ for two-photon resonances; the sign of $i\Gamma$, which is determined by the specific resonant process, can be obtained without calculation, by inspection of diagrams such as were explained in Section III,E. The angle brackets indicate that such singly resonant contributions are to be summed over all species present in a unit volume of the sample. These species may be different molecules or the same molecules in different environments or in different

electronic, vibrational, or rotational (phonon) states. The term χ_{NR} is often a real quantity representing the contribution of all nonresonant transitions for which the frequency mismatch is much larger than the damping parameter.

In four-wave mixing experiments, the intensity of the coherently generated light is measured as a function of $\{\omega_l\}$. The light intensity is proportional to the square of the nonlinear source polarization (see Section III.D): thus it measures $|\chi^{(3)}|^2$, which is the sum of the squares of the real and imaginary parts of Eq. (65). For an isolated resonance, the signal will show a maximum and a minimum when

$$\omega_{ab} + \{\omega_l\} = \pm[(A_{ab}/2\chi_{NR})^2 + \Gamma_{ab}^2]^{1/2} - A_{ab}/2\chi_{NR} \tag{66}$$

The variation with frequency of a susceptibility of this type thus leads to the determination of resonance frequencies ω_{ab}, the corresponding damping parameter Γ_{ab}, and the amplitude of the resonance measured with respect to the nonresonant background A_{ab}/χ_{NR}.

C. Raman and Two-Photon Resonances in Four-Wave Mixing

Many experimental studies of singly resonant responses have involved Raman and two-photon resonances using $\chi^{(3)}$, the lowest-order susceptibility to which these resonances contribute. Four-wave mixing, arising from two different input frequencies ω_1 and ω_2 and monitored by the intensity of light generated by the induced polarization at $\omega_3 = 2\omega_1 - \omega_2$, has emerged as a versatile method of measuring singly resonant $\chi^{(3)}$ in gases, liquids, and solids. The frequencies of all light beams involved in this situation are similar, and phase matching is therefore easy to achieve in all media, yet the directional signal at $2\omega_1 - \omega_2$ is readily isolated. The generated beam can be chosen so that $\omega_3 > \omega_1 > \omega_2$ or that $\omega_3 < \omega_1 < \omega_2$. These Raman resonant contributions were given the acronyms CARS and CSRS, for coherent anti-Stokes (or Stokes) Raman scattering/spectroscopy. When χ_{NR} is real, both methods lead to the same spectral shapes for a given resonant level pair, but when two-photon and Raman resonances interfere, the CARS and CSRS spectra will differ because the signs of the damping parameters in Eq. (65) are different for CARS and CSRS.

In spontaneous Raman spectroscopy with conventional monochromators, the spectral resolution is about 0.2 cm^{-1}. Improvements can be accomplished by means of elaborate interferometric methods. In contrast, the spectral resolution in CARS is determined by the spectral bandwidth of the lasers. It was therefore natural to use CARS for high-resolution gas-phase Raman spectroscopy and to probe the chemical composition and the temperature

distribution within flames (Regnier and Taran, 1973; Regnier *et al.*, 1974; Moya *et al.*, 1975). The generation of light at the anti-Stokes frequency is resonance-enhanced when $\omega_1 - \omega_2$ matches a vibrational frequency and also when there are two-photon resonances. It follows from Eq. (43) and Eq. (45) that the polarization in a medium displaying both Raman and two-photon effects takes the form

$$P^{(3)} = \langle \chi_{NR} + R_{ab}/(\omega_{ab} + \omega_1 - \omega_2 - i\Gamma_{ab}) + T_{ad}/(\omega_{ad} + 2\omega_1 - i\Gamma_{ad}) \rangle \quad (67)$$

The amplitudes R_{ab} and T_{ad} of the Raman and two-photon resonances, respectively, are directly related to Raman scattering and two-photon absorption cross sections and are readily calibrated in these experiments. The comparatively low probability of two-photon absorption processes has resulted in the development of many indirect detection methods, but it is often not practical to use such techniques to determine absolute cross sections. Absolute Raman cross sections, on the other hand, have been measured for a number of molecules and, as Raman resonances are fairly narrow even at room temperatures, have been used in organic liquids and solids to determine $\chi^{(3)}$ (Levenson and Bloembergen, 1974a,b; Hochstrasser *et al.*, 1980). This calibration is in turn used to evaluate the two-photon tensor T_{ad} of individual vibronic lines. In condensed phases the vibrational structure of electronic transitions can only be resolved at low temperatures, and two-photon cross sections of individual vibronic bands can thus only be measured under these conditions. Measurements on single crystals of benzene, naphthalene, and biphenyl are discussed in detail by Hochstrasser *et al.* (1980). The spectra of neat benzene crystals at 1.6 K are shown in Fig. 5: the two-photon fluorescence excitation spectrum obtained by Hochstrasser *et al.* (1973a,b, 1974) is shown together with four wave-mixing spectra for the spectral region around the strongest two-photon transition corresponding to the excitation of a b_{2u} nuclear displacement on the $^1B_{2u}$ excited state surface, the overall two-photon process thus corresponding to a transition between two A_g states. The frequency difference $\omega_1 - \omega_2$ was chosen to be close to the frequency of skeletal modes (around 1600 cm^{-1}; upper trace) and of C—H stretch modes (around 3050 cm^{-1}; lower trace). The continuous line is a fitted spectrum calculated according to Eq. (67). In all three materials it was found that the magnitude of the two-photon tensor of the strongest transitions was similar to the corresponding values for the stronger Raman transitions.

More important than these calibrations of optical constants and transition strengths of single crystals at low temperatures is the fact that, because the coherent signals in these experiments can easily be measured over an extremely large dynamic range, line shapes can be accurately determined with narrow band lasers. Figure 6 shows the CARS spectrum of the pure naphthalene crystal (DeCola *et al.*, 1980b). In this case the stronger Raman

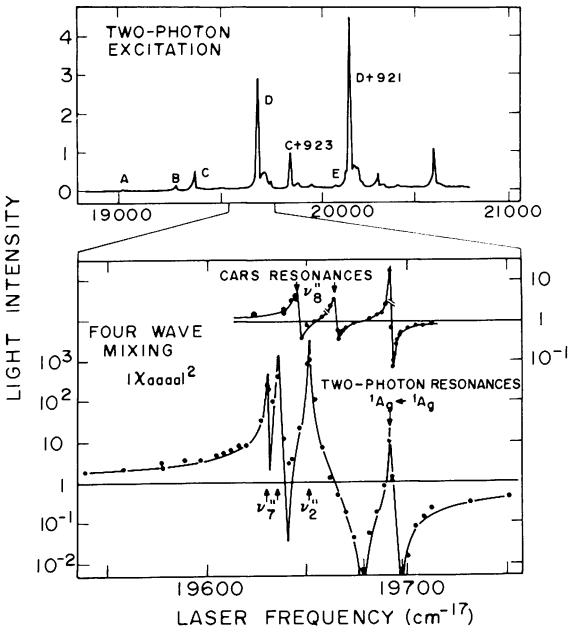

Fig. 5. Two-photon fluorescence (top) and four-wave mixing spectra (bottom) of benzene crystals at 1.6 K. The transition marked D in the top spectrum corresponds to the $14_0^1(A_g)$ band of the ${}^1B_{2u} \leftarrow {}^1A_g$ electronic transition and is the strongest vibronic origin of the two photon spectrum. The same transition is seen in the bottom spectra, together with Raman resonances of ground-state vibrational modes; the frequency of the ω_1 laser is scanned while ω_2 is chosen such that $\omega_1 - \omega_2$ is in the region of C—C and C—H stretch modes, respectively, in the upper and lower traces.

resonance could be fitted to a single Lorentzian line with a Γ of 0.03 cm^{-1} corresponding to an exponential decay constant of 90 psec.

A fundamental issue in the analysis of line shapes in the condensed phase is the separation of inhomogeneous and homogeneous contributions. In the case of the pure crystal of naphthalene, the rapid delocalization of the 1385-cm^{-1} excitation averages out the inhomogeneous frequency distribution. This effect for excitons is analogous to the motional narrowing better known in magnetic resonance. The transition for a static inhomogeneous gaussian distribution to a motionally narrowed Lorentzian line is described in a model developed by Kubo (Kubo and Tomita, 1954; Kubo, 1969) in which the transition frequency is stochastically modulated to yield a response function given by

$$R(t) = \exp\{-\sigma^2\tau_c^2[\exp(-t/\tau_c) - 1 + t/\tau_c]\} \tag{68}$$

Here σ is the gaussian parameter of the frequency distribution and τ_c the correlation time of the stochastic jumps. For a crystal excitation in the

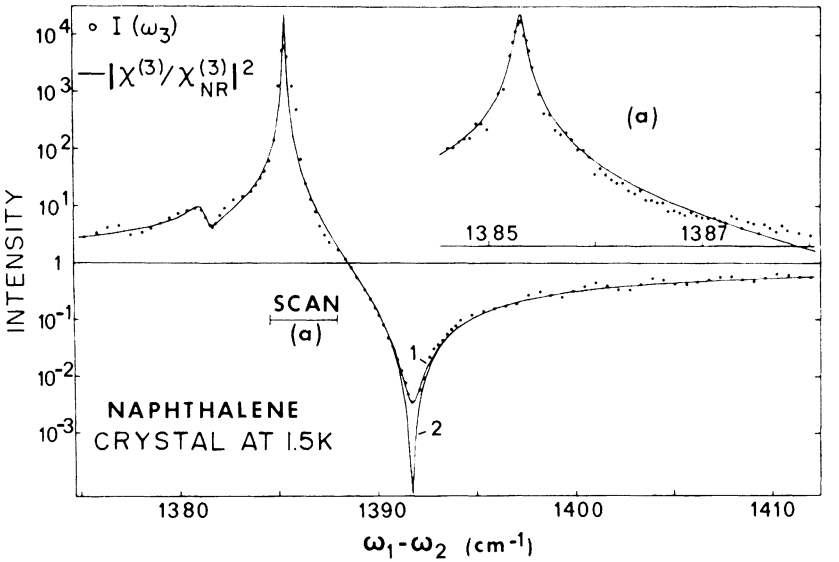

Fig. 6. CARS spectra of a naphthalene single crystal at 1.5 K. The directions of propagation of all beams are nearly perpendicular to the *ab* plane and all polarization are parallel to the *a* axis. The continuous trace was calculated according to Eq. (66) with $\chi_{NR} = |\chi_{NR}|(1 - i\varepsilon)$ where $\varepsilon = 0.05$ in curve 1 and $\varepsilon = 0$ in curve (2); $\omega_1 = 16{,}994\ \text{cm}^{-1}$.

restricted Frenkel limit, τ_c corresponds to the jump time of a localized excitation between neighboring sites and σ is the gaussian width of the inhomogeneous distribution of site energies, as would be measured, for example, in a dilute mixed crystal. When the bandwidth β is small (i.e., τ_c very long), the coherence will decay on a time scale short compared with τ_c (provided that $\sigma\tau_c \gg 1$): in this limit, $R(t) \approx \exp(-\sigma^2 t^2/2)$, and in the frequency domain a gaussian line with the full inhomogeneous width σ is observed. When, on the other hand, $\sigma\tau_c \ll 1$, the decay becomes $R(t) \approx \exp(-\sigma^2 t/\beta)$, corresponding to a Lorentzian line of width σ^2/β: the exciton motion thus reduces the line width by a factor σ/β. A discussion of these points more specifically directed at exciton systems was given by Abram and Hochstrasser (1979). In low-temperature single crystals, the inhomogeneous contribution becomes negligible compared with the lifetime contribution to the line width as a result of this narrowing.

Dynamics of vibrational state relaxation in crystals can also be studied in time-domain experiments in which ω_1 and ω_2 first create the coherence between the $v = 0$ and $v = 1$ levels, and this coherence is probed at a later time by an ω_1 beam. A measurement of the decay of the light field generated at frequency $\omega_3 = 2\omega_1 - \omega_2$ yields the coherence decay parameter Γ for the two-level system. If in time-domain experiments the light intensity is measured, the

observed decay constant is expected to be 2Γ. In the case of the naphthalene crystal 1385-cm^{-1} band, time-domain experiments yielded an exponential decay constant in excellent agreement with the CARS value (Hesp and Wiersma, 1980). Similar comparisons now exist for benzene modes (Ho *et al.*, 1981; Trout *et al.*, 1984). In fact, both time- and frequency-domain experiments measure the same response of the system. This is readily seen by inspection of the form of the CARS response function, R_{CARS}:

$$R_{\mathrm{CARS}} = \sum_{a,v,c,d} \rho_a \exp\{(i\omega_{ac} + \Gamma_{ac})(\tau_1 - \tau_2) + (i\omega_{av} + \Gamma_{av})(\tau_2 - \tau_3) + (i\omega_{ad} + \Gamma_{ad})(\tau_3 - t)\} \tag{69}$$

In the conventional time resolved CARS experiment, $\tau_1 = \tau_2$ (the first two interactions come from pulses that are centered at the same instant). The vibrational levels of the ground state are labelled v. When the fields E_1 and E_2 are in the transparent regime and E_3 is delayed by τ, the CARS signal for nearly δ-function pulses has the form

$$I_{\mathrm{CARS}}(\tau) \sim \mathrm{const}\left|\sum_{a,v} \rho_a \exp(i\omega_{va} - \Gamma_{av})\tau\right|^2 \tag{69b}$$

When the pulses have a finite spectral bandwidth, specific vibrational resonances can be excited, each having the asymptotic intensity decay function $\exp(-2\Gamma_{av}\tau)$. The effect of intermediate pulsewidths is obtained directly from Eqs. (6) and (69). The signal $I_{\mathrm{CARS}}(\tau)$ versus τ is a Fourier transform Raman spectrum. Note that the Fourier transform of Eq. (69), using Eq. (10), is given by Eq. (42). Only in the limit when the duration of the light pulses is much shorter than the coherence decay or when the frequency bandwidth of the laser is much smaller than the width of the resonance are the time and frequency CARS responses simply transforms of one another. In real experiments these conditions are frequently not met, and the spectral–temporal properties of the laser fields have to be convoluted with the system response via Eq. (6) or Eq. (9) in order to simulate properly the observed signals and to extract the physical meaningful parameters (Ho *et al.*, 1983).

Benzene is one of the best understood organic crystals. The 991-cm^{-1} ring-stretching vibration forms an exciton band in the crystal that can be excited in a Raman transition to its lowest-energy Davydov component by proper choice of the light polarization. Figure 7 shows measurements of the coherence decay by picosecond time-resolved CARS for this mode, as well as frequency-domain measurements in benzene crystals of natural isotopic composition: the decay times determined in both types of experiments agree with the error limits.

The study of vibrational linewidths in low-temperature molecular crystals by high-resolution CARS is only a few years old, but a clear picture of certain

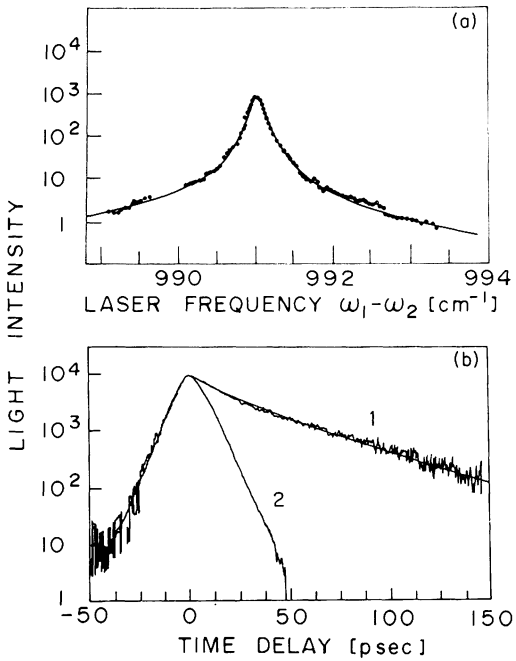

Fig. 7. (a) Frequency and (b) time domain (curve 1) CARS spectra of the ν_1 991-cm^{-1} mode of benzene single crystals of natural isotopic composition. Curve (2) is an instrument function obtained from liquid benzene. The linewidth parameter (0.067 cm^{-1}) obtained from the top spectrum agrees within experimental error with the decay time (40 psec) obtained from the bottom curve.

aspects of coherence decay in these systems begins to emerge. As the temperature of a crystal is lowered, the vibrational linewidth decreases until (around 10 K) it becomes close to a temperature-independent limit. The residual ($T = 0$) linewidth is due to dephasing or energy transfer. From a time-domain point of view, dephasing processes represent mechanisms by which initially well-defined phase relations among the excited oscillators in the wavepacket are randomized by strain fields, or by defect and impurity scattering. This can be pictured as the evolution of a relatively smooth Fourier-limited initial excitation wavepacket into a structure characterized by a correlation length inversely proportional to the width of the distribution of k states into which the wavepacket has evolved. In energy-transfer processes, vibrational amplitude diminishes evenly at all excited sites of the crystal, preserving all initially present phase relationships. This kind of decay is accompanied by the spontaneous emission of phonons and corresponds to a loss of vibrational population from the initially excited mode (T_1 process). In a pure crystal, from which all chemical and isotopic impurities have been

removed, only strain-induced dephasing and lifetime broadening due to spontaneous emission of phonons contribute to the vibrational linewidth.

An important goal of these nonlinear studies of crystals is to learn about molecular relaxation processes. The population decay rates for benzene were found to increase with the total vibrational energy content for benzene as shown in Fig. 8. The benzene crystal is sufficiently harmonic that $\Delta v = \pm 1$ selection rules were expected to determine the relaxation pathways involving both the internal and the external, relative motion, degrees of freedom. An explanation of this trend was recently given in terms of the variations of the anharmonicities of the benzene molecular modes. The internal anharmonicities of the benzene modes are expected to increase with vibrational frequency. At low vibrational energy, say less than 1000 cm^{-1}, there is a harmonic region within which the existence of $\Delta v = \pm 1$ possibilities is not sufficient for a rapid relaxation. In the higher-energy, or "free-access," region, coupling may occur to many of the levels that are separated by less than one lattice-vibrational quantum, as a result of the increased molecular anharmonicities and Fermi resonances. At a certain state density still in the region of the fundamentals, the molecular motions might be sufficiently mixed to allow each mode to relax into many channels while still maintaining the $\Delta v = \pm 1$ selection rule for lattice modes. Internal mode mixing of this nature was also invoked to describe the relaxation of CH stretching modes in liquids (Fendt *et al.*, 1981) specifically in that case in terms of their coupling to CH bending motions.

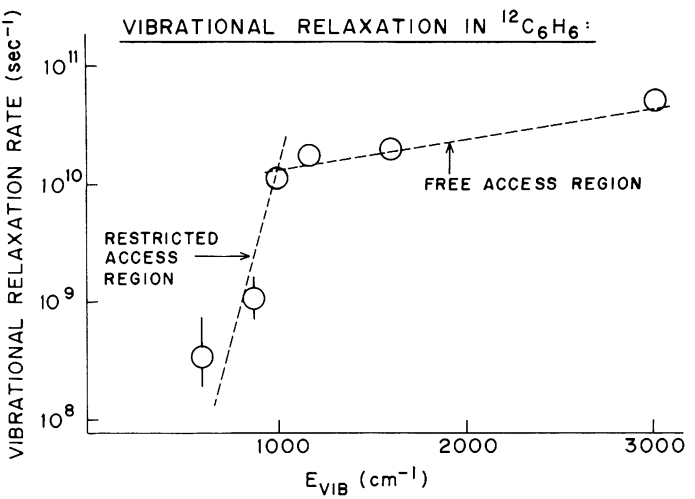

Fig. 8. Vibrational relaxation rates of some Raman-active modes in benzene. The dashed line is intended to draw the eye to the two regions of behavior of rate versus total vibrational energy.

It will be interesting to discover whether the trend of Fig. 8 is upheld by studies of the infrared active modes of benzene and whether these basic ideas carry over to other systems. The energy at which the anharmonic effects become dominant is expected to vary from system to system. For example, in larger molecules where there are many more lower-frequency modes, the onset of the free-access region may be at quite low total energy. The lowest-frequency modes may then be too close to the lattice modes for there to be a significant restricted region.

Molecular crystal vibrational transitions can be extremely sharp and, as a result of the exchange of vibrational energy, can display multiplets (factor group component states) of closely spaced lines. The study of the quantum beats in time-resolved CARS [see Eq. (69b)] was shown by Velsko *et al.* (1983) to be an effective nonlinear method of ultrahigh resolution spectroscopy required to determine the position and widths of these lines. These experiments were carried out with ~ 5 ps pulses, but current femtosecond technology should enable the observation of the beats between and optical pumping of the molecular vibrational states.

As dilute impurities are added (or for neat crystals with natural abundances of isotopic impurities), line-broadening mechanisms due to energy trapping or scattering by impurities become operative. Simple theoretical models indicate that dephasing due to scattering is a slow process, except possibly in the resonant regime, where the impurity levels lie close to the host band. The lineshape for the dilute impurity takes on a form typical of impurity spectra: if the guest level is sufficiently far from nearby host bands, the lineshape will have a strong inhomogeneous component, which reflects the distribution of site energies due to crystal strain fields. The homogeneous component of the line reflects population decay, both to the surrounding host material and to lower modes of the guest molecules. If there is no spectral diffusion, the lineshape will be a convolution of the inhomogeneous and homogeneous bands.

At high doping levels ($\sim 50\%$), a number of processes become interwoven: impurity scattering may make an appreciable contribution to dephasing. The motional narrowing effect is reduced by the dilution of the host structure, allowing strains to contribute an inhomogeneous character to the linewidth. The population decay also changes character, becoming an "incoherent" process. All of these effects are not necessarily separable and additive.

As an example, Fig. 9 shows the CARS lineshape of the ν_1 A_g mode in crystalline benzene for a neat C_6H_6 crystal, for a 50% mixed C_6H_6/C_6D_6 crystal, and for dilute (3%) C_6H_6 in a C_6D_6 host. Note both the nonmonotonic dependence of overall linewidth on concentration and the qualitative change in the lineshapes. One expects different modes to exhibit different behavior, depending on where the $k = 0$ state lies within the band and on how close it lies to the levels of the isotopic diluent. Dlott and co-workers (Chronister and

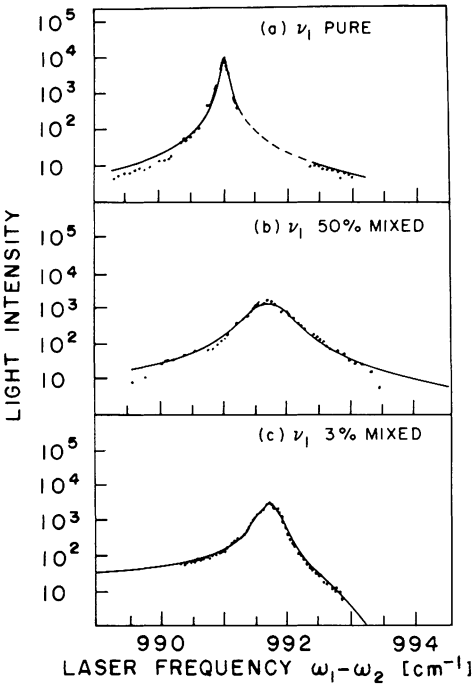

Fig. 9. Dependence of the benzene ν_1 A_g line width on concentration of perproto- in perdeuterobenzene. (a) Isotopically pure crystal with fit to a Lorentzian line shape, $\Gamma = 0.043$ cm^{-1}; the fits in the mixed-crystal spectra (b) and (c) are convolutions of gaussian and Lorentzian line shapes with parameters $\Gamma = 0.13$ cm^{-1}, $\sigma = 0.25$ cm^{-1}, and $\Gamma = 0.073$ cm^{-1}, $\sigma = 0.133$ cm^{-1} for the 50% and 3% crystals, respectively.

Dlott, 1983; Schosser and Dlott, 1984) have studied the concentration dependence of vibrational coherence decay times in mixtures of proto- and perdeuteronaphthalene, and have observed several distinct behaviors for different modes. It is clear that to interpret these dependences it is necessary to know in detail the vibrational levels of the host and guest molecules and their band structures, as well as the intrinsic strain-induced site energy distribution and its dependence on impurity concentration.

Vibrational energy relaxation and energy transfer to impurities are the most "chemically" interesting processes, since they relate to broader questions about vibrational relaxation in molecular systems. There are now a few cases where coherence decay can be unambiguously assigned to these mechanisms. In this respect an important experimental challenge is to make systematic studies of vibrational relaxation in crystals using direct T_1 measurements. Of course, from the point of view of exciton transport theory, dephasing processes are of interest in themselves, and also because of their potential for

affecting the dynamics of population decay processes, especially trapping (Velsko and Hochstrasser, 1985a,b).

D. Resonances in $\chi^{(2)}$

The second-order electric dipole susceptibility was rarely used in spectroscopic applications because it vanishes in centrosymmetric media. Benzene, naphthalene, and anthracene are, as are most molecular crystals, centrosymmetric, and two-photon transitions are therefore allowed only between levels of the same parity. However, in all these materials two-photon transitions were noticed to occur from the totally symmetric ground state to levels known to be of u symmetry from one-photon spectra (Hochstrasser and Sung, 1977b; Hochstrasser *et al.*, 1979). In addition, a resonance-enhanced second-harmonic generation was observed, corresponding again to $g \rightarrow u$ transitions (Hochstrasser and Meredith, 1977, 1978, 1979; Stevenson *et al.*, 1981; Stevenson and Small, 1983). The anisotropic properties of these nonlinear effects suggested a two-photon process in which one photon couples through the electric and the other through the magnetic dipole interaction. In these experiments, fusion of the initially created polaritons generates a polariton at twice the incident laser frequency, which may either result in incoherent light (hyper-Raman scattering) or may survive as a coherent beam at 2ω. The measurements for a crystal of naphthalene are shown in Fig. 10. The sharp angular dependence of the peak of the signal maps the dispersion of the polariton: the generation of the second-harmonic beam is governed by the phase-matching conditions, and as 2ω resonates with a one-photon allowed transition, the index of refraction at this frequency varies rapidly not only as a function of the frequency (polariton dispersion) but also, in these biaxial crystals, as a function of the direction of the wave vector. Similar experiments have also been performed in the noncentric crystal phenanthrene (Johnson and Small, 1982a,b); in this system, transitions to the first electronic state are both one-photon and two-photon allowed and can thus be observed as resonances in $\chi^{(2)}$ and $\chi^{(3)}$. The quantitative analysis of the experimental data is rendered complex in noncentric systems because of interactions between incident and generated fields. In molecular crystals the problem of this cascading in higher-order processes has been critically analyzed by Meredith (1981, 1982). In centrosymmetric crystals these processes do not occur within the electric dipole approximation, and the forbidden second-order processes remain weak: in this case the breaking of the inversion symmetry by defects or by the surface may become important in contributing significantly to the generated signals.

At roughened metal surfaces, optical nonlinearities are strongly enhanced by the local field. This effect is thought to make significant contributions to

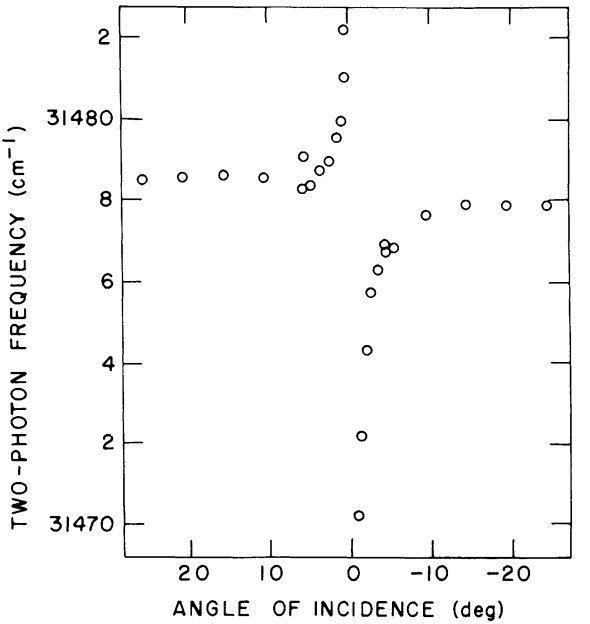

Fig. 10. Variations of maxima of the second-harmonic signal as a function of laser-beam incidence angle in single crystals of naphthalene at 4.2 K. The angle is measured relative to the normal of the *ab* plane and the crystal is rotated about *b*; the polarization of the incident beam is parallel to *b*.

surface-enhanced Raman scattering (SERS). The contribution of adsorbed molecules to second harmonic generation also becomes very large such that molecular monolayers can easily be detected, as was shown by Shen and coworkers (Chen *et al.*, 1981; Heinz *et al.*, 1981, 1982, 1983). Such contributions become large even for centrosymmetric molecules: the second-order polarizability induced in the local field may reach values as large as those observed for polar molecules.

E. Fully Resonant $\chi^{(2)}$

In the presence of a dc electric field, $\chi^{(2)}$ phenomena such as sum- and difference-frequency generation will occur in all media. Although the observed effects are strictly third-order in the applied fields, two optical and one dc, the coherent light generation pathways and the dynamical parts of the susceptibility determining the spectral shapes are characteristic of $\chi^{(2)}$ processes. Using this approach, spectroscopic applications of both sum- and difference-frequency generation under fully resonant conditions have been explored (Dick and Hochstrasser, 1983d, 1984a). The system used to demonstrate these

effects was a mixed crystal of a polar guest (azulene) doped substitutionally into a centrosymmetric host (naphthalene). The average dipole moment of the mixed crystal is zero, but in the presence of a dc electric field the random translational lattice of guest molecules is transformed into two interpenetrating but distinguishable sublattices consisting of polar molecules whose dipoles project parallel and antiparallel to the applied field. The optical transitions of the guest molecules in these two sublattices can then be separately observed. If this system is now subject to an intense electromagnetic field having an arbitrary frequency, it will respond as if it were noncentrosymmetric. Conventional electric-field-induced second-harmonic generation will occur, for example, with the SHG radiation intensity depending on the square of the dc-field strength. However, a qualitatively different effect is observed when the oscillating field is nearly resonant with one of the guest transitions corresponding to just one of the polar sublattices. In this case, the field senses a material that is polar, and at sufficiently high dc fields the $\chi^{(2)}$ process, occuring as a result of the response of one sublattice, becomes nearly independent of the dc field strength. The experiments were carried out with the optical field chosen to be resonant with spectrally sharp transitions of the S_1-S_0 and S_2-S_0 transitions of azulene. The permanent dipole moments of S_0, S_1, and S_2 are known to be sufficiently different that relatively small dc fields cause readily observable pseudo-Stark splittings of the spectral lines and effectively separate the two sublattices. The resonant contribution to $\chi^{(2)}$ of each sublattice separately are given by

$$\chi^{(2)}_{\mathrm{SUM}} = \frac{\mu^{(1)}_{01}\mu^{(2)}_{12}\mu^{(3)}_{20}}{(\omega_{10}-\omega_1+i\Gamma_{01})[\omega_{20}-(\omega_1+\omega_2)+i\Gamma_{02}]} \tag{70}$$

$$\chi^{(2)}_{\mathrm{DIF}} = \frac{\mu^{(2)}_{20}\mu^{(1)}_{01}\mu^{(3)}_{12}}{(\omega_{10}-\omega_1+i\Gamma_{01})(\omega_{20}-\omega_2-i\Gamma_{02})}\left\{1+\frac{i(\Gamma_{12}-\Gamma_{01}-\Gamma_{02})}{[\omega_{21}-(\omega_2-\omega_1)-i\Gamma_{12}]}\right\} \tag{71}$$

Resonances should therefore occur at ω_{10} and ω_{20} in both sum and difference frequency generation, and in addition a resonance at ω_{12} is predicted in the presence of pure dephasing (DICE resonance; see Section IV,G). In zero field, the contributions of the two sublattices have equal absolute values but are of opposite sign and cancel. In a dc field the shift of the transition frequencies ω_{ij} is opposite for the two sublattices, resulting in a net nonzero value of $\chi^{(2)}$, which can be obtained from Eqs. (70) and (71) as

$$\chi = \chi(\omega_{ij} - \Delta\boldsymbol{\mu}_{ij}\cdot\mathbf{F}) - \chi(\omega_{ij} + \Delta\boldsymbol{\mu}_{ij}\cdot\mathbf{F}) \tag{72}$$

where $\Delta\boldsymbol{\mu}_{ij}$ is the difference of permanent dipole moment of azulene in states i and j, and F the electric field strength along $\Delta\boldsymbol{\mu}$. Since the naphthalene host

crystal is centrosymmetric, the nonresonant field induced value of $\chi^{(2)}$ is very small and can be neglected. This predicted behavior of $\chi^{(2)}$ is manifested in the experiment. Figure 11 shows examples of the field-induced sum- and difference-frequency generation signal; all predicted resonances except the DICE resonance are observed in these experiments, and the change of shape as a function of field strength can be fitted by formulas for $\chi^{(2)}$ as obtained from Eqs. (70)–(72). The absence of the DICE resonance was rationalized by numerical calculations of the spectra using parameters derived from linear spectroscopic data, which predict it to be more than three orders of magnitude weaker than the main resonance and to be thus unobservable under the experimental conditions. The ω_{20} and ω_{10} resonances appear very similar in the sum- and difference-frequency spectra, although complementary line-narrowing properties are predicted for both spectra. This is because the purely homogeneous contribution to the nonlinear linewidth dominates and any

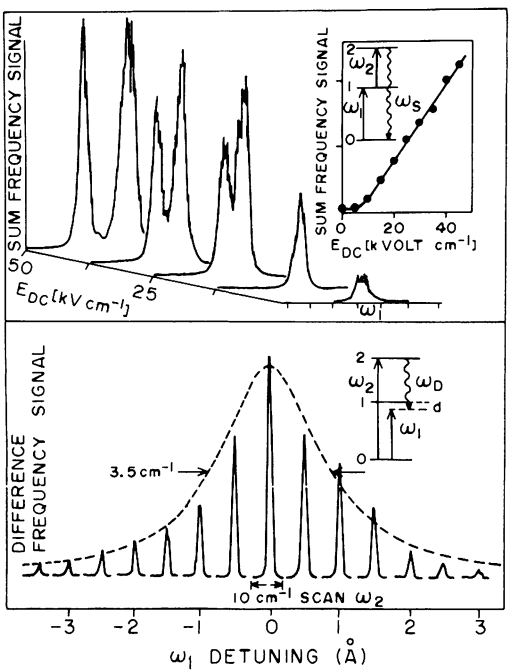

Fig. 11. Resonant sum- and difference-frequency generation of mixed crystals of azulene in naphthalene in an applied electric field. Top: Sum-frequency spectra for increasing dc field strength in the c' direction. Insert: The peak intensity of a sum-frequency signal as a function of dc field strength for low fields. Bottom: Difference-frequency generation in a dc field of 50 kV/cm along c' for various detunings of ω_1. The broken line is a fitted Lorentzian that maps the line shape of the $S_0 \rightarrow S_1$ transition.

correlations within the inhomogeneous contributions have only a slight effect in this case. In systems where the inhomogeneous width dominates, these experiments can be used for line narrowing and to study inhomogeneous correlations, as described in Section III.G and also discussed in the next section.

F. Four-Level Systems and Fully Resonant $\chi^{(3)}$

In order that a general four-wave mixing process be fully resonant, the system must have four levels, and each of these levels must be connected to two other levels by a one-photon allowed transition (see Fig. 3). This condition is very naturally met in molecules when the fundamental frequencies are in the range of electronic or vibronic transitions and when their differences equal vibrational or rotational frequencies. With only two different incident laser beams, just two resonance conditions can, in general, be fullfilled simultaneously, but in molecular systems a third resonance is also met approximately in as far as vibrational frequencies in different electronic states are usually similar (see 3–6 in Fig. 3). With use of three tunable input frequencies, exact resonance can of course be achieved for all possible transitions. The susceptibility of a medium of noninteracting molecules is proportional to the number density, and the measured signals are proportional to $|\chi|^2$. For a fully resonant four-level system, however, the susceptibility may become very large and not only allow the study of extremely dilute samples ($\sim 10^{-2}$ ppm) but also make it possible to address and study specific molecular species in selected states and/or environments.

The first fully resonant four-wave mixing studies were done in the dilute mixed crystal system of pentacene dispersed in benzoic acid (DeCola *et al.*, 1980a). The host, benzoic acid, forms high-quality crystals that are transparent not only to the visible frequencies ω_1 and ω_2 but also to $2\omega_1$ and $2\omega_2$. This system is expected to correspond closely to the theoretical model that treats two monochromatic waves at ω_1 and ω_2 coupled to a four-level system having resonances near $\omega_2, \omega_1, \omega_1 - \omega_2$, and $2\omega_1 - \omega_2$. The four levels correspond to the zeropoint levels (0 and 0′) of ground and excited states and any pair of vibrational levels v and u', chosen from each of these states, for which $\mu_{vu'}$ is nonzero. The case where $v = u$, so that the same mode is involved in each state, was studied in detail.

Figure 12 shows experiments where ω_1 is fixed at the 0–0 transition, ω_2 tuned in the region of the fluorescence lines, and the generated beam at $2\omega_1 - \omega_2$ is monitored. The resonantly enhanced signals can be many times stronger than those from the host material, notwithstanding the fact that the observed light intensity varies with the square of the concentration. For this

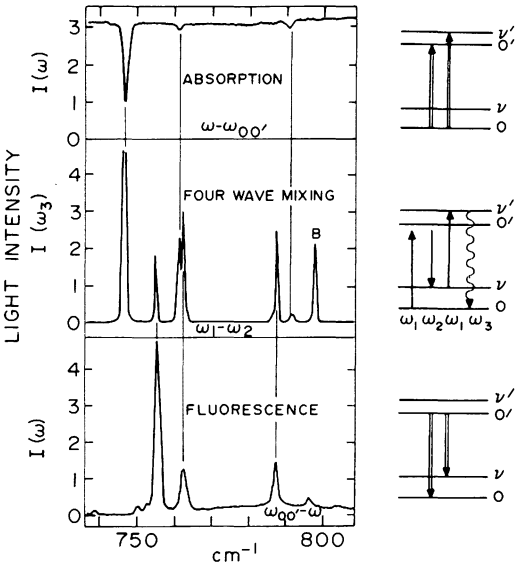

Fig. 12. Absorption, fluorescence, and CARS four-wave mixing spectra of pentacene in a benzoic acid crystal at 1.6 K. The four-wave mixing spectrum was measured on a crystal of 5×10^{-7} mol/mol concentration, and ω_1 was in exact resonance with the 0–0 transition of pentacene. The band B is a benzoic acid CARS resonance and can be used for calibration of the signal since it has a conventional off-resonance Raman cross section comparable with the 992 cm^{-1} mode of benzene.

case the enhancement factor was found to be greater than 10^{15}! The four-wave mixing signal is seen to contain information from both absorption and emission spectroscopy. Actually, the resonant part of the homogeneous response in this case takes the form

$$\sum_{u,v} \frac{(1/\Gamma_{00'})\mu_{00'}\mu_{0'v}\mu_{vu'}\mu_{u'0}}{[i(\omega_{u'} - \Delta) - \Gamma_{u'0}][i(\omega_v - \Delta) - \Gamma_{v0}]} \tag{73}$$

where ω_v and $\omega_{u'}$ are ground- and excited-state vibrational frequencies corresponding to modes v and u and $\Delta = \omega_1 - \omega_2$. The signal is the square of this function with peaks at $\Delta = \omega_v$ and $\Delta = \omega_{u'}$ for all modes u and v for which transition momonts in the numerator exist. For many molecules, however, the dominant contribution comes from $v = u$. This results from the fact that $\mu_{vu'}$ is often maximum when $u = v$, especially in large molecule spectra. In addition, $\omega_v - \omega_{v'}$ is frequently small. Indeed, intense signals are obtained from modes that have nearly the same frequency in the ground and excited states since then both factors in the denominator of Eq. (73) become small at about the same value of Δ. An example, shown in Fig. 12, is the mode at $\omega_v = 762$, $\omega_{v'} = 761$

cm^{-1}, which shows only a weak absorption line but a relatively strong doublet in the coherent experiment. The states u' and v must correspond to the same chemical component of the system, otherwise $\mu_{vu'} = 0$. Thus this technique can be used to identify the occurence of different components in a mixture, different sites such as in mixed crystals, and matrix-isolated species or different aggregates of the same species. An example of the last case is the identification of the levels of dimers of pentacene in a host crystal of *p*-terphenyl. These pairs are observed at higher doping levels, e.g., 10^{-4} to 10^{-3}, and correspond to situations where two neighboring *p*-terphenyl host molecules are replaced by a pair of pentacene guests. The ratio of pairs to isolated monomers is proportional to the doping level and remains therefore very small under usual conditions. Each excited state of the monomer gives rise to three levels of the dimer, two singly excited levels (plus and minus combinations of the molecular excitations) and one doubly excited level. Linear spectroscopic methods do not expose the dimer transitions, which are buried under the monomer absorption. Using the high selectivity of fully resonant four-wave mixing, Levinsky and Wiersma (1982) have been able to locate all these levels for one dimer. Of particular interest is the fact that the resonance associated with the doubly excited level is fairly narrow, corresponding to a lifetime of at least 2 psec, for the relaxation of this state by excitation fusion.

G. DICE Effects

There are three fully resonant time orderings that contribute to the generation of steady-state Stokes radiation in a four-level system, as indicated in Fig. 13. The second diagram differs from the first in that the initial ω_1 field is interchanged in time with the ω_2 field. Both these processes involve introducing coherence in a level pair $v'0'$ (the excited-state Raman transition). Generally, when coherence is introduced into a pair of levels, the response function will exhibit a resonance at the transition frequency. While each of the two terms in Fig. 13 resonate on $\omega_{v'} = \omega_2 - \omega_1$, it turns out that the sum of these terms need not display this resonance. In fact, this excited-state Raman resonance is predicted to be absent if the quantity $\Gamma = \Gamma_{00'} + \Gamma_{0v'} - \Gamma_{0v'}$ is exactly zero. This is the case when the pure dephasing (elastic) parts of the coherence decay vanish. The response as a function of $\Delta = \omega_2 - \omega_1$ is given approximately by

$$(\omega_{v'} + d - \Delta + i\Gamma_{0v'})^{-1}[(\omega_v - \Delta + i\Gamma_v)^{-1} + \Gamma(\omega_{v'} - \Delta + i\Gamma_{v'})^{-1}(\omega_v - d - \Delta - i\Gamma_{0'v})^{-1}] \tag{74}$$

The absolute square of this function yields resonances at $\omega_{v'} + d$ and $\omega_v - d$, both of which have electronic transition widths, and resonances at ω_v and $\omega_{v'}$

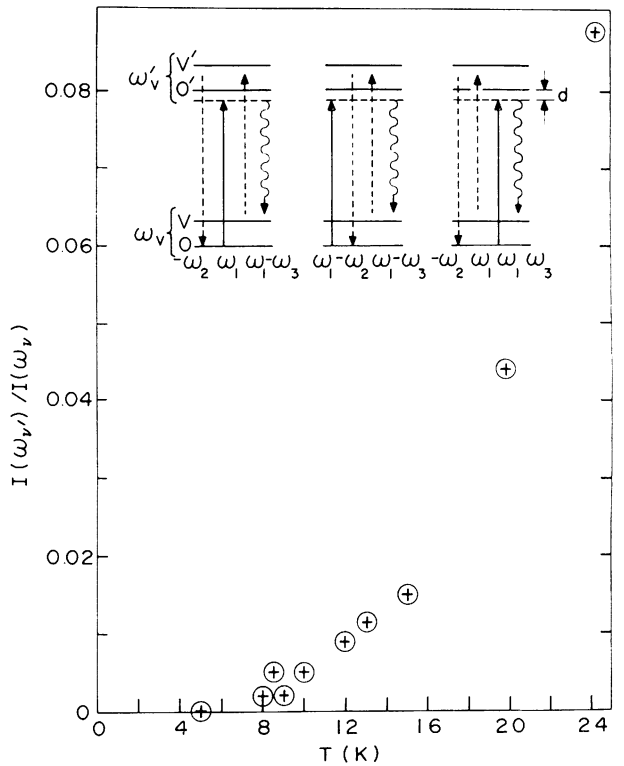

Fig. 13. Ratio of the signal intensity at $\Delta\omega = \omega_{v'}$ (747 cm^{-1}) and $\Delta\omega = \omega_v$ (755 cm^{-1}) in coherent Stokes Raman spectra as a function of temperature for pentacene in a benzoic acid crystal. The relevant diagrams for both resonances are inserted and are discussed in the text.

having the Raman widths of each of the electronic states. This interesting prediction implies that in the condensed phase at near the absolute zero of temperature where the pure dephasing might be small, one may expect little or no enhancement of the Stokes signal from the condition $\omega_2 - \omega_1 = \omega_{v'}$. On the other hand, at finite temperatures the excited-state Raman process is predicted to appear. This effect is termed dephasing induced coherent emission (DICE) (Andrews and Hochstrasser, 1981a,b). From the standpoint of spectroscopy it has important consequences, since inter-excited-state transitions can be studied without first *populating* the excited states. The populations are introduced by pure dephasing, or collisional redistribution in gases, in the same process that converts Raman scattering into fluorescence emission. The predicted temperature effects bring forth a method to measure directly the pure dephasing of transitions. Other coherent techniques such as photon echoes and hole-burning spectroscopy measure only the total dephasing rate.

The results for Stokes generation using pentacene in benzoic acid are given in Fig. 13. The DICE effect growth of intensity at the resonance condition $\omega_2 - \omega_1 = \omega_{v'}$ compared with that at $\omega_2 - \omega_1 = \omega_v$ is attributed to the onset of pure dephasing in the system. DICE processes are, in fact, accounted for in the usual form of the resonant susceptibility (Bloembergen *et al.*, 1978) and were recently seen also in atomic vapors as a PIER-4 effect (Prior *et al.*, 1981).

A question inherent in these experiments concerns the contribution of excited-state populations to the generated signal. In fact, the same dephasing process that brings about the DICE signal converts the polarization into population. This question was investigated by Bozio *et al.* (1983) by measuring CARS and CSRS spectra as a function of detuning d. At 1.6 K and 4.2 K and for small values of d (<5 cm^{-1}), the spectra show resonances at $|\omega_1 - \omega_2| = \omega_{v'}$ independent of d, demonstrating the buildup of excited-state population during the laser pulse. In the DICE experiment discussed above, d was large enough (16.8 cm^{-1}) and the contribution of the excited-state populations to the observed signals were estimated to be negligible. However, line broadening at higher temperatures makes population buildup possible for larger detuning, but comparisons of CARS and CSRS studies allow in this case the identification of the DICE effect (Andrews *et al.*, 1981).

The nonlinear responses of these four-level systems were also studied directly in time-domain experiments (Duppen *et al.*, 1983). The two Stokes diagrams 5 and 6 in Fig. 3, which give rise to the DICE resonance in quasi-cw (continuous wave) experiments can, in principle, be separated in time-domain studies with light pulses that are short compared with the system relaxation times. The time behavior corresponding to these two diagrams is

$$\exp[-(i\omega_{ac} + \Gamma_{ac})(t_1 - t_2) - (i\omega_{dc} + \Gamma_{dc})(t_2 - t_3) - (i\omega_{bc} + \Gamma_{bc})t_3] \quad (75)$$

$$\exp[-(i\omega_{da} + \Gamma_{da})(t_1 - t_2) - (i\omega_{dc} + \Gamma_{dc})(t_2 - t_3) - (i\omega_{bc} + \Gamma_{bc})t_3] \quad (76)$$

where in Eq. (75) a pulse at ω_2 arrives at $t_1 = t - \tau_1 = 0$ resonant or near resonant with the $a \rightarrow c$ transition, while in Eq. (76) ω_1 arrives at $t = \tau_1$ near resonant with the $a \rightarrow d$ transition. For the case where the ω_1 and ω_2 pulses arrive together, $\tau_1 = \tau_2$, a probe pulse at ω_2 generates Stokes light whose intensity variation with pulse delay, $\tau = \tau_3 - \tau_2 = t_2 - t_3$, measures the excited-state dynamics Γ_{cd}. The response function for both diagrams becomes in this case the same and is equal to

$$R(t) = -i\mu_{ac}\mu_{da}\mu_{bd}\mu_{cb}\exp[-(i\omega_{bc} + \Gamma_{bc})(t - \tau)]\exp[-(i\omega_{dc} + \Gamma_{dc})\tau] \quad (77)$$

The integrated intensity of the signal generated at ω_{bc} is equal to

$$I(\tau) = c\int_{\tau}^{\infty} dt_3 |R(t_3)|^2 = I_0 e^{-2\Gamma_{dc}\tau} \quad (78)$$

with $I_0 = c/2\Gamma_{bc}$ being the intensity of the signal for $\tau = 0$. Notice that this experiment does not depend on the existence of pure dephasing, so that the DICE effect is seen to be a result of averaging over times long compared with the relaxation dynamics.

One interesting aspect of these fully resonant processes is their potential for exploring inhomogeneous distributions (see Section III.G). For the 755/747 cm^{-1} mode of bentacene in benzoic acid at 1.6 K, it was found that the width of the ground state Raman resonance is about two times smaller in CARS than in CSRS spectra (Bozio *et al.*, 1983). This is a clear indication of the fact that the inhomogeneous distributions of the ground-state Raman and the electronic transitions are anticorrelated: that is, molecules absorbing at the higher frequency side of the 0–0′ band center contribute to the lower-energy portion of the inhomogeneous ground-state vibrational transition at 755 cm^{-1}.

H. Grating Experiments

As the frequency difference between the incident laser beams becomes smaller, lower-frequency molecular modes and optical and eventually acoustical phonons are probed. In fact, these experiments probe in general phenomena occuring on the timescale of $1/\Delta\omega$. These coherent Rayleigh mixing experiments have been used to probe dynamical processes in liquids (Yajima *et al.*, 1976, 1978; Yajima and Souma, 1978; Heilweil *et al.*, 1980; Souma *et al.*, 1982). The way in which these experiments probe the dynamics can be envisioned by considering the spatial distribution of light intensity set up in the sample by two intersecting incident beams: for two beams of equal frequency ω and field strength E crossing in the sample at an angle of 2θ, the intensity in the sample is spatially periodic

$$|E_1 + E_1'|^2 = 4E^2 \cos^2(2\pi y \sin\theta/\lambda) \tag{79}$$

corresponding to a stationary diffraction grating along the direction y that is parallel to $\mathbf{k}_1 - \mathbf{k}_1'$. Another beam ω_2 will diffract from this grating with the overall process leading to the generation of a beam at ω_2 in the direction $\mathbf{k}_1 - \mathbf{k}_1' + \mathbf{k}_2$. It is easy to see that this corresponds to the Bragg diffraction condition for a grating having the character of Eq. (79). When the frequencies of the two beams creating the grating differ by an amount $\Delta\omega = \omega_1 - \omega_2$, the spatial intensity distribution is no longer stationary and the diffracted beam will be Doppler shifted by an amount $\Delta\omega$. The diffraction of ω_1 gives rise to light emitted at frequency $2\omega_1 - \omega_2$. The amplitude of the grating and therefore the intensity of the diffracted beam is determined by the variation of the refractive index of the medium that is induced by

the incident E_1 fields. Different contributions to this variation stem from thermal, population, and coherence transfer processes, and these contributions build up and decay with different characteristic time constants. In a moving grating, therefore, only contributions with characteristic time constants faster than $1/\Delta\omega$ will show up: otherwise they will be washed out. Thus, the dynamics of the medium can be probed by varying the frequency difference of the two beams creating the grating. For example, with incident visible beams separated by 1 cm^{-1}, processes occuring on the time scale of 5 psec are singled out.

The time-domain analogue of these moving-grating experiments are the so-called transient-grating experiments. In these experiments, two time-coincident laser pulses of the same frequency are crossed in the sample and produce a grating, which is probed by a delayed third pulse. The grating represents a spatially periodic modulation of the index of refraction, which has contributions from the population of excited electronic or vibrational states or phonons (or more generally of other species produced in the excitation process such as electron–hole pairs, for example, in semiconductors) and due to modulations of the density of the material produced by periodic heating or directly by electrostriction. The buildup of the grating amplitude occurs over a finite time and its observation permits study of the kinetic processes contributing to it. The probe pulse need not be of the same frequency as the excitation pulses and can be chosen to be resonant with a different transition and thereby to enhance specific contributions to the grating. In molecular crystals, transient-grating experiments have been used to study excited-state lifetimes, excited state absorptions, and exciton transport properties (Eichler, 1977; Fayer, 1982, 1983; Rose *et al.*, 1984).

Transient gratings have also been used to stimulate ultrasonic waves and to measure their speed and attenuation (Nelson *et al.*, 1982); these experiments correspond to Brillouin scattering in the time domain and are particularly useful when the attenuation becomes very large and difficult to measure in the frequency domain. For example, this method was employed to follow soft modes near a phase transition (Robinson *et al.*, 1984).

In transparent media the coupling to the light field occurs by electrostriction, but the generation of coherent acoustic phonons in optically absorbing media is more readily achieved by impulsive heating. These techniques to generate and monitor ultrasonic waves are superior to conventional methods, especially when the properties of the material make it difficult to establish a good mechanical contact with a transducer, or when the acoustic attenuation becomes so high that the wave is damped over only a few cycles. These situations arise frequently when a material undergoes interesting structural transformations: in polymer materials, for example, the glass transition as a function of temperature or the transformation from monomer to polymer

during the polymerization may be studied using these methods, as is illustrated in Fig. 14 (Blanchard *et al.*, 1985).

Transient-grating experiments are intimately related to stimulated photon echo experiments: they correspond to the limit in which the time difference between the first two pulses in the echo experiment goes to zero. The situation in which the state of the grating is probed by a different color corresponds to two-color photon echo experiments (Duppen *et al.*, 1984a,b). Both experiments probe the same physical processes, namely the evolution of the population of the levels connected by the light fields.

I. Molecular Reorientation

The populations of excited states generated by nonlinear optical interactions are usually anisotropic. This anisotropy is manifested as a dichroism. Nonlinear signals that depend on such dichroism have response functions that

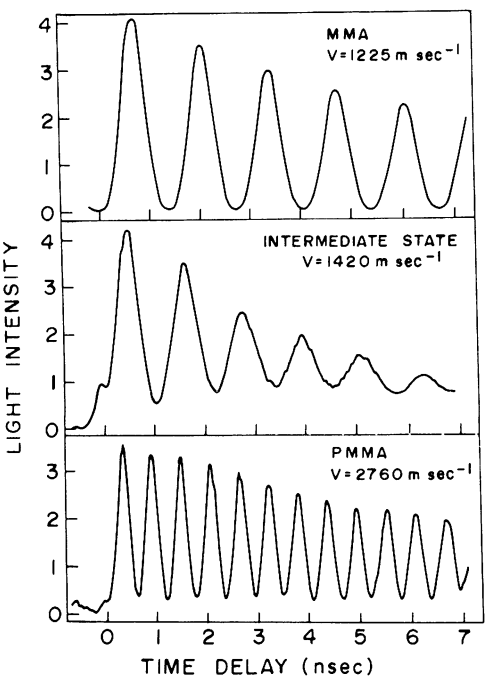

Fig. 14. Time evolution of a standing ultrasonic wave generated by impulsive heating by two time-coincident crossed laser pulses in methylmethacrylate during polymerization. While the speed of sound increases monotonically during this process, the acoustic attenuation becomes very large and passes through a maximum at an intermediate state of polymerization.

decay on the reduced time scale of T_1 relaxation and the orientational correlation time of the transition dipoles that generate the resonances. One example of such a signal is found in the polarization spectroscopy of molecules in solutions (Shank and Ippen, 1975; Reiser and Laubereau, 1982; Cross *et al.*, 1983; Myers and Hochstrasser, 1986). Motional properties of systems are usefully described using the conventional susceptibilities in cases where the motion is slow compared with the electromagnetic field impulses and T_2 decay times. In that case the response function of the system is developed by iteration in the usual way, except that the transition dipole factor is taken to be time-dependent but slowly varying (Myers and Hochstrasser, 1986).

For a system of four levels, a and b coupled by the excitation fields 1 and 2 at time 0, c and d coupled by the probing field, 3, at time τ, the usual density matrix expansion yields a slowly varying portion of the response to linear polarized fields having the form

$$\langle \boldsymbol{\mu}_{ab}(0) \cdot \hat{\mathbf{e}}_1 \boldsymbol{\mu}_{ba}(0) \cdot \hat{\mathbf{e}}_2 \boldsymbol{\mu}_{cd}(\tau) \cdot \hat{\mathbf{e}}_3 \boldsymbol{\mu}_{dc}(\tau) \cdot \hat{\mathbf{e}}_4 \rangle = |\mu_{ab}\mu_{cd}|^2 (A + Be^{-\tau/\tau_R}) \quad (80)$$

where $\hat{\mathbf{e}}_4$ is the polarization of the generated wave. This response refers to all experiments involving a field product $\mathscr{E}_1 \mathscr{E}_1^* \mathscr{E}_2$, including polarization spectroscopy, transient gratings, and crossed gratings. Conventional Bragg diffraction in which a transient grating formed by excitation pulses of the same polarization ($\hat{\mathbf{e}}_1 \cdot \hat{\mathbf{e}}_2 = 1$) is probed with parallel ($\hat{\mathbf{e}}_3 \cdot \hat{\mathbf{e}}_2 = 1$) and perpendicular ($\hat{\mathbf{e}}_3 \cdot \hat{\mathbf{e}}_2 = 0$) polarizations has the advantage of yielding both the time dependence and the magnitude of the induced anisotropy. However, the accompanying acoustic grating interferes with the polarization-sensitive excited-state grating. In the crossed-grating configuration, the acoustic signal is eliminated by the use of perpendicularly polarized excitation pulses $\hat{\mathbf{e}}_1 \cdot \hat{\mathbf{e}}_2 = 0$ Polarization spectroscopy ($\hat{\mathbf{e}}_1 \cdot \hat{\mathbf{e}}_2 = 0$; $\hat{\mathbf{e}}_4 \cdot \hat{\mathbf{e}}_3 = 0$) gives the same susceptibility and anisotropy dynamics as the crossed grating but is more sensitive to interference from background birefringence because $\mathbf{k}_4 = \mathbf{k}_3$.

The orientation average of Eq. (80) is readily evaluated for the case of isotropic diffusion having relaxation time τ, to yield the following values for the constants A and B:

$A = \frac{1}{3}$;	$B = 2r_0/3$	for conventional grating probed parallel
$A = \frac{1}{3}$;	$B = -r_0/3$	for crossed grating probed perpendicular
$A = 0$;	$B = r_0/2$	for crossed grating and polarization spectroscopy

where $r_0 = \frac{2}{5}\langle P_2[\boldsymbol{\mu}_{ab}(0) \cdot \boldsymbol{\mu}_{cd}(\tau)]\rangle$ and P_2 is the second Legendre polynomial. It is easy to deduce the relative signal intensities (at time zero) for each of these techniques. The results are given in Table I. These techniques are each useful in determining rotational relaxation dynamics in molecular condensed phases. Furthermore, when the four waves all have the same frequency, the methods

TABLE I

Angular Averages and Relative Signal Strengths for Different Four-Wave Mixing Configurations

	Ordinary grating, parallel probe[a]	Ordinary grating, perpendicular probe[a]	Crossed grating	Polarization spectroscopy
$\hat{\mathbf{e}}_1\hat{\mathbf{e}}_2\hat{\mathbf{e}}_3\hat{\mathbf{e}}_4$	$zzzz$	$zzyy$	$zyzy$[b]	$zz(z+y)(z-y)\frac{1}{2}$
$\langle\mu_i^{(1)}(0)\mu_i^{(2)}(0)\mu_j^{(3)}(T)\mu_j^{(4)}(T)\rangle$[c]	$\frac{1}{3}(1+2r_0e^{-T/\tau_R})$	$\frac{1}{3}(1-r_0e^{-T/\tau_R})$	$\frac{1}{2}r_0e^{-T/\tau_R}$	$\frac{1}{2}r_0e^{-T/\tau_R}$
Signal at $T=0$ for $\hat{\boldsymbol{\mu}}_i\cdot\hat{\boldsymbol{\mu}}_j=1$	9	1	1	4
Signal at $T=0$ for $\hat{\boldsymbol{\mu}}_i\cdot\hat{\boldsymbol{\mu}}_j=0$	1	4	0.25	1

[a] The field polarization and angular averages for fluorescence with parallel and perpendicular detection are the same as for the ordinary grating. The parallel : perpendicular signal ratios for fluorescence are the square root of those for the grating.

[b] In the crossed grating, any choice of $\hat{\mathbf{e}}_3$ gives the same signal strength. In general, if $\hat{\mathbf{e}}_3=\cos\theta\hat{\mathbf{z}}+\sin\theta\hat{\mathbf{y}}$, then $\hat{\mathbf{e}}_4=\sin\theta\hat{\mathbf{z}}+\cos\theta\hat{\mathbf{y}}$.

[c] Assuming isotropic rotational diffusion with time constant τ_R; $r_0=\frac{2}{5}\langle P_2[\hat{\boldsymbol{\mu}}_i\cdot\hat{\boldsymbol{\mu}}_j]\rangle$.

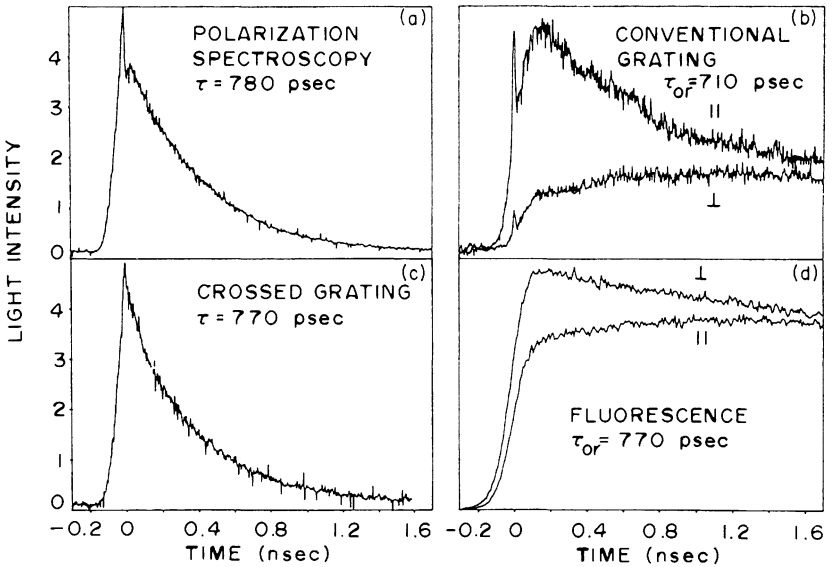

Fig. 15. Comparison of different techniques measuring the rotational relaxation dynamics of 9-aminoacridine in ethylene glycol. The excitation wavelength in all experiments is 266 nm. In (a)–(c), the coherence introduced in the sample is probed with a time-delayed pulse of the same frequency. For comparison in (d), the incoherent fluorescence of the sample detected at right angles at 460 nm is also shown. The difference of the two signals in (c) and (d) should measure the same dynamical process as each of the signals in (a) and (b).

provide a way of measuring T_2 for the pumped transition through studies of the "coherent spike" seen at zero delay time (see Fig. 15).

Figure 15 shows the experimental results for 9-aminoacridine using each of the grating configurations discussed above. The signal in each case corresponds to the square of the response function in Eq. (80). The deduced value of $\tau_R = 760 \pm 20$ psec obtained from each experiment corresponds in this case to the rotation of the molecule about an axis perpendicular to the molecular plane.

V. SUMMARY AND PROGNOSIS

This article was intended to provide an overview of nonlinear optical studies of molecular systems with particular emphasis on molecular condensed matter spectroscopic applications. We have shown that a wide range of material parameters can be determined by means of either time or frequency domain experiments that employ tunable lasers. The use of multiple laser

fields allows the study of double or triple resonance effects and of dynamical processes involving molecular and excitonic excited states. The nonlinear optical theory provides the framework on which to understand all such multiresonant phenomena including induced emission, absorption, and spontaneous decay.

For the future, there are a number of obvious directions that resonant molecular optics is likely to take. First, there is the study of extremely rapid responses using femtosecond light pulses more closely approximating those of Eq. (7). Recently, the coherent Raman beating implicit in Eq. (69) and observed for benzene using picosecond pulses (Velsko *et al.*, 1983) was studied with femtosecond pulses by Nelson and coworkers (De Silvestri *et al.*, 1985). In addition it seems very interesting to proceed with the study of systems not close to equilibrium. This situation might involve materials that are heavily ionized or highly concentrated in excited states or excitons and systems in which a large fraction of certain atoms, for example protons, are displaced from their equilibrium configurations. Another area of great interest barely touched on in this article is surface molecular optics. It is apparent that the principles presented here can be used to make detailed studies of surface states and of dynamical processes involving adsorbed molecules. Finally, an important area is the development and characterization of new molecular materials having the required resonances and dynamics to permit qualitative improvements in, as well as the generation of, new types of optical materials.

ACKNOWLEDGMENTS

This research was supported by grants from NSF, NIH, AROD, and the LRSM Program at Pennsylvania. We are indebted to our colleagues in the Penn Molecular Optics group for their contributions and encouragement.

REFERENCES

Abram, I., and Hochstrasser, R. M. (1979). *In* "Light Scattering in Solids" (J. L. Birman, ed.), p. 447. Plenum, New York.

Abram, I., and Hochstrasser, R. M. (1980). *J. Chem. Phys.* **72,** 3617.

Allen, L., and Eberly, J. H. (1975). "Optical Resonance and Two-Level Atoms." Wiley, New York.

Andrews, J. R., and Hochstrasser, R. M. (1981a). *Chem. Phys. Lett* **82,** 381.

Andrews, J. R., and Hochstrasser, R. M. (1981b). *Chem. Phys. Lett.* **83,** 427.

Andrews, J. R., Hochstrasser, R. M., and Trommsdorff, H. P. (1981). *Chem. Phys.* **62,** 87.

Bechtel, I. H., and Smith, W. L. (1976). *Phys. Rev. B* **13,** 3515.

Blanchard, D., Casalegno R., Pierre, M., and Trommsdorff H. P. (1985). *J. Phys.* **46,** C7–517.

Bloembergen, N. (1965). "Nonlinear Optics." Benjamin, New York.

Bloembergen, N., Lotem, H., and Lynch, R. T., Jr. (1978) *Indian J. Pure Appl. Phys.* **16,** 151.
Bordé, C. J. (1976). *C. R. Hebd. Seances Acad. Sci., Ser. B* **282,** 341.
Bordé, J., and Bordé, C. J. (1978). *J. Mol. Spectrosc.* **78,** 353.
Bozio, R., DeCola, P. L., and Hochstrasser, R. M. (1983). *In* "Time-Resolved Vibrational Spectroscopy" (G. H. Atkinson, ed.), p. 335. Academic Press, New York.
Burns, M. J., Lin, W. K., and Zewail, A. H. (1983). *In* "Spectroscopy and Excitation Dynamics of Condensed Molecular Systems" (V. M., Agranovich, and R. M., Hochstrasser, eds.), p. 301. North-Holland Publ., Amsterdam.
Burris, J., McGee, T. J., and McIlrath, T. J. (1983). *Chem. Phys. Lett.* **101,** 588.
Butcher, P. N. (1965). "Nonlinear Optical Phenomena." Ohio State University Engineering Publications, Columbus.
Chen, C. K., Heinz, T. F., Richard, D., and Shen, Y. R. (1981). *Phys. Rev. Lett.* **46,** 1010.
Chronister, E. L., and Dlott, D. D. (1983). *J. Chem. Phys.* **79,** 5286.
Cross, A. J., Waldeck, D. H., and Fleming, G. R. (1983). *J. Chem. Phys.* **78,** 6455.
Davydov, A. S. (1971). "Theory of Molecular Excitons," Plenum, New York.
DeCola, P. L., Andrews, J. R., Hochstrasser, R. M., and Trommsdorff, H. P. (1980a). *J. Chem. Phys.* **73,** 4695.
DeCola, P. L., Hochstrasser, R. M., and Trommsdorff, H. P. (1980b). *Chem. Phys. Lett.* **72,** 1.
De Silvestri, S., Fujimoto, J. G., Ippen, E. P., Gamble, E. B., Jr., Williams, L. R., and Nelson, K. A. (1985). *Chem. Phys. Lett.* **116,** 146.
De Vries, H., and Wiersma, D. A. (1976). *Phys. Rev. Lett.* **36,** 91.
Dick, B., and Hochstrasser, R. M. (1983b). *J. Chem. Phys.* **78,** 3398.
Dick, B., and Hochstrasser, R. M. (1983b). *Chem. Phys.* **75,** 133.
Dick, B., and Hochstrasser, R. M. (1983c). *Chem. Phys. Lett.* **102,** 484.
Dick, B., and Hochstrasser, R. M. (1983d). *Phys. Rev. Lett.* **51,** 2221.
Dick, B., and Hochstrasser, R. M. (1984a). *Chem. Phys.* **91,** 1.
Dick, B., and Hochstrasser, R. M. (1984b). *J. Chem. Phys.* **81,** 2897.
Druet, S. A. J., Attal, B., Gustafson, T. K., and Taran, J. P. E. (1978). *Phys. Rev. A* **18,** 1529.
Duppen, K., Weitekamp, D. P., and Wiersma, D. A. (1983). *J. Chem. Phys.* **79,** 5835–5844.
Duppen, K., Weitekamp, D. P., and Wiersma, D. A. (1984a). *Chem. Phys. Lett.* **106,** 141.
Duppen, K., Weitekamp, D. P., and Wiersma, D. A. (1984b). *Chem. Phys. Lett.* **108,** 551.
Eichler, E. J. (1977). *Opt. Acta* **24,** 431.
Fayer, M. D. (1982). *Annu. Rev. Phys. Chem.* **33,** 631.
Fayer, M. D. (1983). *In* "Spectroscopy and Excitation Dynamics of Condensed Molecular Systems," (V. M. Agranovich and R. M. Hochstrasser, eds.), p. 185 North-Holland Publ., Amsterdam.
Fendt, A., Fischer, S. F., and Kaiser, W. (1981). *Chem. Phys.* **57,** 55.
Flytzanis, C. (1975). *In* "Quantum Electronics: A Treatise" (H. Rabin and C. L. Tang, eds.), Vol. 1A, Part A, p. 1. Academic Press, New York.
Heilweil, E. J., Hochstrasser, R. M., and Souma, H. (1980). *Opt. Commun.* **35,** 227.
Heinz, T. F., Chen, C. K., Richard, D., and Shen, Y. R. (1981). *Chem. Phys. Lett.* **83,** 180.
Heinz, T. F., Chen, C. K., Richard, D., and Shen, Y. R. (1982). *Phys. Rev. Lett.* **48,** 478.
Heinz, T. F., Tom, H. W. K., and Shen, Y. R. (1983). *Phys. Rev. A* **28,** 1883.
Hellwarth, R. W. (1977). *Prog. Quantum Electron* **5,** 1.
Hesp, B. H., and Wiersma, D. A. (1980). *Chem. Phys. Lett.* **75,** 423.
Hesselink, W. H., and Wiersma, D. A. (1983). *In* "Spectroscopy and Excitation Dynamics of Condensed Molecular Systems" (V. M. Agranovich and R. M. Hochstrasser, eds.), p. 249. North-Holland Publ., Amsterdam.
Ho, F., Tsay, W. S., Trout, J., and Hochstrasser, R. M. (1981). *Chem. Phys. Lett.* **83,** 5.
Ho, F., Tsay, W. S., Trout, J., Velsko, S., and Hochstrasser, R. M. (1983). *Chem. Phys. Lett.* **97,** 141.

Hochstrasser, R. M. (1973). *Acc. Chem. Res.* **6,** 263.
Hochstrasser, R. M. (1976). *Int. Rev. Sci.: Phys. Chem., Ser. 2* **3,** 1.
Hochstrasser, R. M., and McAlpine, R. D. (1966). *J. Chem. Phys.* **44,** 3325.
Hochstrasser, R. M., and Meredith, G. R. (1977). *J. Chem. Phys.* **67,** 1273.
Hochstrasser, R. M., and Meredith, G. R. (1978). *Pure Appl. Chem.* **50,** 759.
Hochstrasser, R. M., and Meredith, G. R. (1979). *J. Luminescence* **18/19,** 32.
Hochstrasser, R. M., and Sung, H. N. (1977a). *J. Chem. Phys.* **66,** 3265.
Hochstrasser, R. M., and Sung, H. N. (1977b). *J. Chem. Phys.* **66,** 3276.
Hochstrasser, R. M., Sung, H. N., and Wessel, J. E. (1973a). *J. Am. Chem. Soc.* **95,** 8179.
Hochstrasser, R. M., Sung, H. N., and Wessel, J. E. (1973b). *J. Chem. Phys.* **58,** 4694.
Hochstrasser, R. M., Wessel, J. E., and Sung, H. N. (1974). *J. Chem. Phys.* **60,** 317.
Hochstrasser, R. M., Klimcak, C. M., and Meredith, G. R. (1979). *J. Chem. Phys.* **70,** 870.
Hochstrasser, R. M., Meredith, G. R., and Trommsdorff, H. P. (1980). *J. Chem. Phys.* **73,** 1009.
Hudson, B. S., Kohler, B. E., and Schulten, K. (1982). *In* "Excited States" (E. C. Lim, ed.), Vol. 6, p. 1. Academic Press, New York.
Johnson, C. K., and Small, G. J. (1982a). *J. Chem. Phys.* **76,** 3837.
Johnson, C. K., and Small, G. J. (1982b). *Chem. Phys.* **64,** 83.
Klafter, J; and Jortner, J. (1977). *Chem. Phys. Lett.* **50,** 202.
Klafter, J., and Jortner, J. (1978). *J. Chem. Phys.* **68,** 1513.
Kubo, R. (1969). *Adv. Chem. Phys.* **15,** 101.
Kubo, R., and Tomito, K. (1954). *J. Phys. Soc. Jpn.* **9,** 888.
Levenson, M. D., and Bloembergen, N. (1974a). *J. Chem. Phys.* **60,** 1323.
Levenson, M. D., and Bloembergen, N. (1974b). *Phys. Rev. B* **10,** 4447.
Levinsky, H., and Wiersma, D. A. (1982). *Chem. Phys. Lett.* **92,** 24.
Liptay, W. (1974). *In* "Excited States" (E. C. Lim, ed.), Vol. 1, p. 129. Academic Press, New York.
Lotem, H., and Lynch, R. T., Jr. (1976), *Phys. Rev. Lett.* **37,** 334.
Lynch, R. T., Jr., and Lotem, H. (1977), *J. Chem. Phys.* **66,** 1905.
McAlpine, R. D. (1968). Ph.D. Dissertation, University of Pennsylvania, Philadelphia.
McClain, W. M., and Harris, R. A. (1977). *In* "Excited States" (E. C. Lim, ed.), Vol. 3. Academic Press, New York.
Meredith, G. R. (1981). *J. Chem. Phys.* **75,** 4317.
Meredith, G. R. (1982). *J. Chem. Phys.* **77,** 5863.
Moya, F., Druet, S. A. J., and Taran, J. P. E. (1975). *Opt. Commun.* **13,** 169.
Mulliken, R. S., and Person, (1969). "Molecular Complexes." Wiley, New York.
Myers, A. B., and Hochstrasser (1986). *IEEE J. Quantum Electron.* **QE22,** 1482.
Nelson, K. A., Casalegno, R., Miller, R. J. D., and Fayer, M. D. (1982). *J. Chem. Phys.* **77,** 1144.
Oudar, J.-L., and Shen, Y. R. (1980), *Phys. Rev. A* **22,** 1141.
Prior, Y., Bogdan, A. R., Dagenais, M., and Bloembergen, N. (1981). *Phys. Rev. Lett.* **46,** 111.
Rabi, I. I. (1937). *Phys. Rev.* **51,** 652.
Regnier, P., and Taran, J. P. E. (1973). *Appl. Phys. Lett.* **23,** 240.
Regnier, P., Moya, F., and Taran, J. P. E. (1974). *AIAA J.* **12,** 826.
Reiser D., and Laubereau, A. (1982). *Chem. Phys. Lett.* **92,** 297.
Righini, K., Fracassi, P. F., and Della Valle, K. G. (1983). *Chem. Phys. Lett.* **97,** 308.
Robinson, G. W. (1970). *Ann. Rev. Phys. Chem.* **21,** 429.
Robinson, M. M., Yan, Y.-X., Gamble, E. B., Jr., Williams, L. R., Meth, J. S., and Nelson, K. A. (1984). *Chem. Phys. Lett.* **112,** 491.
Rose, T. S., Righini, R., and Fayer, M. D. (1984). *Chem. Phys. Lett.* **106,** 13.
Schmalz, T. G., and Flygare, W. H. (1978). *In* "Laser and Coherence Spectroscopy" (J. I. Steinfeld, ed.), pp. 125–196. Plenum, New York.
Schosser, C. L., and Dlott, D. D. (1984). *J. Chem. Phys.* **80,** 1394.

Shank, C. V., and Ippen, E. P. (1975). *Appl. Phys. Lett.* **26,** 62.
Shen, Y. R. (1974). *Phys. Rev. B* **9,** 622.
Small, G. J. (1983). *In* "Spectroscopy and Excitation Dynamics of Condensed Molecular Systems" (V. M. Agranovich and R. M. Hochstrasser, eds.), p. 515. North-Holland Publ., Amsterdam.
Souma, H., Heilweil, E. J., and Hochstrasser, R. M. (1982). *J. Chem. Phys.* **76,** 5693.
Stevenson, S. H., and Small, G. J. (1983). *Chem. Phys. Lett.* **100,** 334.
Stevenson, S. H., Johnson, C. K., and Small, G. J. (1981). *J. Phys. Chem.* **85,** 2709.
Trout, T. J., Velsko, S., Bozio, R., DeCola, P. L., and Hochstrasser, R. M. (1984). *J. Chem. Phys.* **81,** 4746.
Velsko, S., and Hochstrasser, R. M. (1985a). *J. Phys. Chem.* **89,** 2240.
Velsko, S., and Hochstrasser, R. M. (1985b). *J. Chem. Phys.* **82,** 2180.
Velsko, S., Trout, J., and Hochstrasser, R. M. (1983). *J. Chem. Phys.* **79,** 2114.
Whiteman, J., McAlpine, R. D., and Hochstrasser, R. M. (1973). *J. Chem. Phys.* **58,** 5078.
Yajima, T., and Souma, H. (1978). *Phys. Rev. A* **17,** 309.
Yajima, T., Souma, H., and Ishida, Y. (1976). *Opt. Commun.* **18,** 150.
Yajima, T., Souma, H., and Ishida, Y. (1978). *Phys. Rev. A* **17,** 324.
Yee, S. Y., and Gustafson, T. K. (1978). *Phys. Rev. A* **18,** 1597.
Yee, S. Y., Gustafson, T. K., Druet, S. A. J., and Taran, J. P. E. (1977). *Opt. Commun.* **23,** 1.